FILE COPY

TECHNICAL REPORT ARBRL-TR-02422

(Supersedes IMR No. 744)

PRESSURE MOMENT ON A LIQUID-FILLED PROJECTILE: SOLID BODY ROTATION

Nathan Gerber
Raymond Sedney
Joan M. Bartos

October 1982

US ARMY ARMAMENT RESEARCH AND DEVELOPMENT COMMAND
BALLISTIC RESEARCH LABORATORY
ABERDEEN PROVING GROUND, MARYLAND

Destroy this report when it is no longer needed.
Do not return it to the originator.

Secondary distribution of this report is prohibited.

Additional copies of this report may be obtained from the National Technical Information Service, U. S. Department of Commerce, Springfield, Virginia 22161.

The findings in this report are not to be construed as an official Department of the Army position, unless so designated by other authorized documents.

The use of trade names or manufacturers' names in this report does not constitute indorsement of any commercial product.

UNCLASSIFIED

SECURITY CLASSIFICATION OF THIS PAGE *(When Data Entered)*

REPORT DOCUMENTATION PAGE		READ INSTRUCTIONS BEFORE COMPLETING FORM
1. REPORT NUMBER Technical Report ARBRL-TR-02422	2. GOVT ACCESSION NO.	3. RECIPIENT'S CATALOG NUMBER
4. TITLE *(and Subtitle)* PRESSURE MOMENT ON A LIQUID-FILLED PROJECTILE: SOLID BODY ROTATION		5. TYPE OF REPORT & PERIOD COVERED Final 6. PERFORMING ORG. REPORT NUMBER
7. AUTHOR(s) N. Gerber, R. Sedney, and J.M. Bartos		8. CONTRACT OR GRANT NUMBER(s)
9. PERFORMING ORGANIZATION NAME AND ADDRESS U.S. Army Ballistic Research Laboratory ATTN: DRDAR-BLL Aberdeen Proving Ground, Maryland 21005		10. PROGRAM ELEMENT, PROJECT, TASK AREA & WORK UNIT NUMBERS RDT&E 1L161102AH43
11. CONTROLLING OFFICE NAME AND ADDRESS US Army Armament Research & Development Command US Army Ballistic Research Laboratory (DRDAR-BL) Aberdeen Proving Ground, Maryland 21005		12. REPORT DATE October 1982 13. NUMBER OF PAGES 65
14. MONITORING AGENCY NAME & ADDRESS*(if different from Controlling Office)*		15. SECURITY CLASS. *(of this report)* UNCLASSIFIED 15a. DECLASSIFICATION/DOWNGRADING SCHEDULE

16. DISTRIBUTION STATEMENT *(of this Report)*

Approved for public release, distribution unlimited.

17. DISTRIBUTION STATEMENT *(of the abstract entered in Block 20, if different from Report)*

18. SUPPLEMENTARY NOTES

Supersedes IMR No. 744, dated May 1982

19. KEY WORDS *(Continue on reverse side if necessary and identify by block number)*

Liquid Payload	Stewartson-Wedemeyer Theory
Liquid-Filled Shell	Spinning Nutating Cylinder
Liquid-Filled Gyroscope	Rotating Fluid
Liquid Pressure Moment	Linearized Navier-Stokes Equations

20. ABSTRACT *(Continue on reverse side if necessary and identify by block number)*

The liquid-produced moment on a liquid-filled spinning cylinder executing angular motion is determined, where the liquid originally is in solid-body rotation. In an approximation to free-flight spiraling motion of a projectile, the cylinder is nutating at constant frequency about a point on its axis and is undergoing timewise exponential yaw growth. The assumption of small yaw angle permits the formulation of a linearized viscous flow problem as a perturbation

DD FORM 1 JAN 73 1473 EDITION OF 1 NOV 65 IS OBSOLETE

UNCLASSIFIED

SECURITY CLASSIFICATION OF THIS PAGE *(When Data Entered)*

on solid-body rotation. The pressure obtained from the resulting linearized flow is used to obtain the moment. Moment due to shear stresses is not considered. This moment is incorporated into the dynamical equations of gyroscopic motion to determine yaw growth rate and nutational frequency.

This report provides a presentation of the equations and computational procedures. The approach is to apply a modal analysis in the flow solution which gives rise to ordinary differential equations, and then to make a correction required to compensate for neglect of the no-slip conditions at the endwalls in the modal analysis.

Results are compared with those of other theoretical work and with experimental data for endwall pressure, pressure moment, and yaw growth rate of projectiles and gyroscopes. In general, results agree well for high Reynolds number ($>50{,}000$). Relative discrepancies are more prominent at low Reynolds numbers, particularly in yaw growth rate data. Qualitative agreement of present results with concurrent theoretical work of Murphy appears to be consistently good.

TABLE OF CONTENTS

LIST OF ILLUSTRATIONS

I. INTRODUCTION

Current Army investigation of projectiles containing chemical payloads and smoke/incendiary agents has generated new interest in liquid-filled shell. These often exhibit flight behavior different from that of solid-payload projectiles because of an overturning moment exerted by the liquid on the casing. In fact, this liquid moment has produced instabilities which are absent for solid-payload shell.

The work of Stewartson[1], which assumed inviscid flow, and the viscous corrections of Wedemeyer[2,3] have provided the basis of the theoretical predictions made heretofore. This theory applies to liquids in solid-body rotation in projectiles flying with small yaw. It demonstrates the existence of oscillations in the liquid and predicts possible instability when resonance occurs; i.e., when the frequency of angular motion (nutation) of the shell, τ,* is equal to a liquid eigenfrequency (natural frequency of free oscillation), C_R.

The Stewartson-Wedemeyer theory yields values for several liquid parameters in the region of resonance: frequency and damping of free oscillations, and liquid pitch (in plane) and yaw (out of plane) moments. The predictions of this theory have been generally substantiated by gyroscope experiments[4].

The Stewartson-Wedemeyer theory assumes that the timewise variation of the flow variables everywhere in the container is the same as that of the nutational motion. This assumption, applicable for stability studies, would only be valid for actual shell late in the flight, after the fluid has been fully spun-up and coned-up; i.e., liquid transients have decayed. This assumption will be retained in the present work, yielding a time-independent problem.

---

* *Definitions are given in List of Symbols, p. 41.*

1. *K. Stewartson, "On the Stability of a Spinning Top Containing Liquid," Journal of Fluid Mechanics, Vol. 5, Part 4, September 1959, pp. 577-592.*

2. *E. H. Wedemeyer, "Dynamics of Liquid-Filled Shell: Theory of Viscous Corrections to Stewartson's Stability Problem," BRL Report 1287, June 1965. AD 472474.*

3. *E. H. Wedemeyer, "Viscous Corrections to Stewartson's Stability Criterion," BRL Report 1325, June 1966. AD 489687.*

4. *R. Whiting and N. Gerber, "Dynamics of a Liquid-Filled Gyroscope: Update of Theory and Experiment," BRL Technical Report ARBRL-TR-02221, March 1980. AD A083886.*

Previously a theory[5] was developed that uses the linearized Navier-Stokes equations to obtain the free oscillations of the fluid. A modal analysis resulted in an eigenvalue problem for C_R and the decay rate of the waves, C_I. The complexity of this eigenvalue problem requires a large scale computer program. A major part of this program is also required in the present problem which studies the forced oscillations resulting from projectile nutation. The results should be more accurate than those of the Stewartson-Wedemeyer theory, which employs inviscid flow equations plus viscous corrections at sidewall and endwalls.

This work addresses the task of calculating liquid moment by an extension of the above-mentioned procedure[5]. The method is to solve the internal flow problem, calculate the liquid moment by integrating the computed pressure, and then obtain the resultant motion from the dynamical equations of yaw. This study will treat only the case of the completely-filled shell. The moment due to viscous shear will be reported separately. The approach is similar to that of Reference 5; namely, to apply a modal analysis (separation of variables) in the flow solution which gives rise to ordinary differential equations, and in the process making a correction required to compensate for neglect of the no-slip conditions at the endwalls in the modal analysis.

The results of the present analysis will be compared with experimental results whenever possible and with theoretical results of Murphy[6]. The latter uses Wedemeyer's viscous corrections at both sidewall and endwalls to resolve Stewartson's equations.

Some nomenclature that has been used regularly in the past[2-5,7] will now be supplanted by nomenclature from Reference 6.

II. EQUATIONS OF YAWING MOTION

We shall limit our consideration to straight trajectories and small yaw angles. We introduce two coordinate systems. The first is an inertial, earth-fixed system of axes x, y, z. The x-axis coincides with the projectile velocity vector, and the z-axis lies in the vertical plane; then the y-axis is directed so as to form a right-handed system. The second system is the aero-ballistic $\tilde{x}$, $\tilde{y}$, $\tilde{z}$ non-rolling system which has the $\tilde{x}$-axis along the projectile axis of symmetry and the $\tilde{z}$-axis initially in the vertical plane. These systems are shown in Figure 1; the $\tilde{y}$ and $\tilde{z}$ axes are omitted for clarity.

---

5. *C. W. Kitchens, Jr., N. Gerber, and R. Sedney, "Oscillations of a Liquid in a Rotating Cylinder: Part I. Solid-Body Rotation," BRL Technical Report ARBRL-TR-02081, June 1978. AD A057759.*

6. *C. H. Murphy, "Angular Motion of a Spinning Projectile with a Viscous Liquid Payload," BRL Technical Report in preparation.*

7. *Engineering Design Handbook, Liquid-Filled Projectile Design, AMC Pamphlet 706-165, April 1969. AD 853719.*

The $x = 0$ and $\tilde{x} = 0$ values are located at the midplanes of the unyawed and yawed cylinders, respectively. The $\tilde{x}$-axis is nutating about the x-axis at the angle $K_1 = K_1(t)$. The components of the projection in the y, z plane of a unit vector lying on the $\tilde{x}$-axis are denoted by n_{YE} and n_{ZE}.

The yawing motion is characterized by two variables, $\tilde{\alpha}$ and $\tilde{\beta}$. The angle of attack, $\tilde{\alpha}$, in the aeroballistic system is the angle in the vertical plane measured also from the $\tilde{x}$-axis to the velocity vector; the angle of slideslip, $\tilde{\beta}$, is the angle in the horizontal plane measured also from the $\tilde{x}$-axis to the velocity vector. For the small yaw angles considered, $\tilde{\alpha} \simeq -n_{ZE}$ and $\tilde{\beta} \simeq -n_{YE}$. It is convenient to combine $\tilde{\alpha}$ and $\tilde{\beta}$ into a single complex variable:

$$\tilde{\xi} \equiv \tilde{\beta} + i\tilde{\alpha} \simeq -(n_{YE} + i\, n_{ZE}). \tag{1}$$

The fluid pressure forces on the cavity surfaces produced by the motion give rise to a moment on the projectile. The spin-decelerating component, $M_{L\tilde{X}}$, is zero here; the other components can be represented in complex form, $M_{L\tilde{Y}} + iM_{L\tilde{Z}}$. We shall consider only the liquid moment acting on the projectile. The resulting model is adequate for comparing theoretical outputs; the liquid moment can be added to the other moments acting on shell or gyroscrope as required. The differential equation of yawing motion is *

$$I_y\, d^2\tilde{\xi}/dt^2 - i\dot{\phi}I_x\, d\tilde{\xi}/dt + I_y\, \hat{M}\tilde{\xi} = i\,(M_{L\tilde{Y}} + iM_{L\tilde{Z}}). \tag{2}$$

The quantity I_x is the moment of inertia of the empty axisymmetric shell about its longitudinal axis. I_y is the traverse moment of inertia of the empty shell about its center of gravity. The spin rate of the shell is $\dot{\phi}$ (taken to be positive); t is time. The term $I_y\hat{M}\tilde{\xi}$ is an aerodynamic moment for a projectile. For a gyroscope this term is a gravitational moment arising from the separation of center of gravity and pivot point, and in most experiments is zero.

In general there is an interaction between the motion of the projectile and the liquid motion. Here we shall specify the motion of the projectile. In particular the cylinder is nutating with constant frequency and exponentially-growing yaw:

$$\tilde{\xi} = (K_0 e^{\epsilon\tau\dot{\phi}t})e^{i(\tau\dot{\phi}t)} = K_1 e^{i\phi_1} = K_0 e^{if\dot{\phi}t}, \tag{3}$$

---

* *This is Eq. (2.4) of Reference 6 with only the liquid moment on the right-hand side.*

where

$$K_1 \equiv K_0 e^{\varepsilon\tau\dot{\phi}t}, \qquad \phi_1 \equiv \tau\dot{\phi}t, \qquad f \equiv (1-i\varepsilon)\tau. \tag{4}$$

Here K_0 is the magnitude of the yaw at time t = 0; τ is the nutational frequency divided by $\dot{\phi}$, and the yaw grows when $\varepsilon\tau > 0$. Also K_1 is the yaw amplitude, and ϕ_1 is the angular orientation* of the $\bar{X}$-axis in the x, y, z system as shown in Figure 1.

The motion of the projectile enters the flow problem via the boundary conditions. Under the assumption that the flow is in phase with the motion of the shell, the pressure disturbance will have the time dependence of Eq. (3), and consequently the liquid moment will also have this form. A nondimensional liquid moment coefficient, C_{LM}, is now defined**:

$$M_{L\tilde{Y}} + i\, M_{L\tilde{Z}} = m_L\, a^2\dot{\phi}^2\, \tau\, C_{LM}\, K_1 e^{i\phi_1}, \tag{5}$$

where m_L is the mass of the liquid. C_{LM} is a complex quantity whose real part represents a moment that changes the yaw angle, and whose imaginary part changes the nutation rate. Thus:

$$C_{LM} \equiv C_{LSM} + i\, C_{LIM}, \tag{6}$$

where C_{LSM} and C_{LIM} represent the "liquid side moment" and "liquid in-plane moment", respectively. That C_{LSM} and C_{LIM} represent these moments can be demonstrated by taking the scalar products of the moment vector ($M_{L\tilde{Y}}$, $M_{L\tilde{Z}}$) with a unit vector parallel to the yaw vector, (cos ϕ_1, sin ϕ_1), and a unit vector normal to the yaw vector, (- sin ϕ_1, cos ϕ_1), respectively.

III. FLOW PROBLEM

A. Flow Equations and Boundary Conditions

Cylindrical polar coordinates are introduced in the earth-fixed frame

$$y = r\cos\theta, \qquad z = r\sin\theta, \qquad x = x, \tag{7}$$

---

* *For simplicity the angle of attack is assumed to be initially zero and the angle of sideslip to be initially positive; i.e., ϕ_{10} of Reference 6 is zero.*

** *See Eq. (2.7) in Reference 6.*

and in the non-rotating aeroballistic frame,

$$\tilde{y} = \tilde{r} \cos \tilde{\theta}, \qquad \tilde{z} = \tilde{r} \sin \tilde{\theta}, \qquad \tilde{x} = \tilde{x}. \tag{8}$$

All the above terms are non-dimensional; lengths and distances are non-dimensionalized by a, the cross-sectional radius of the cylinder. The relationship between the two sets of cylindrical coordinates for small K_0, obtained from the orthogonal transformation between $\tilde{x}$, $\tilde{y}$, $\tilde{z}$ and x, y, z, is

$$r = \tilde{r} - K_1 (\tilde{x}-\ell) \cos (\phi_1-\tilde{\theta}) + O (K_0^2) \tag{9a}$$

$$\theta = \tilde{\theta} - K_1 [(\tilde{x}-\ell)/\tilde{r}] \sin (\phi_1-\tilde{\theta}) + O (K_0^2) \tag{9b}$$

$$x = \tilde{x} + K_1 \tilde{r} \cos (\phi_1-\tilde{\theta}) + O (K_0^2), \tag{9c}$$

where ℓ is the non-dimensional x-coordinate of the pivot point.

To obtain the flow, we assume a small disturbance to a basic flow, which is taken to be solid-body rotation in an unyawed cylinder. The Navier-Stokes equations are linearized to produce the perturbation equations.* The flow variables are the radial, azimuthal, and axial velocity components, and pressure, given here in non-dimensional form:

$$u = U - K_0 \overset{*}{u}, \qquad v = V - K_0 \overset{*}{v}, \qquad w = W - K_0 \overset{*}{w}, \qquad p = P - K_0 \overset{*}{p}. \tag{10}$$

The symbols u, v, w, and p represent the total values. U, V, W, and P are the basic undisturbed variables; and $\overset{*}{u}$, $\overset{*}{v}$, $\overset{*}{w}$, and $\overset{*}{p}$ are perturbation variables** of order one. For solid body rotation the basic flow is

$$U = 0, \qquad V = r, \qquad W = 0, \qquad \partial P/\partial r = r. \tag{11}$$

The velocity components are non-dimensionalized by $a\dot{\phi}$, and pressure by $\rho a^2 \dot{\phi}^2$, where ρ is the density of the liquid.

On substituting Eqs. (10) and (11) into the Navier-Stokes equations and linearizing with respect to K_0, we obtain the perturbation equations in non-dimensional form:

---

* *These are Eq. (3) in Reference 5.*

** *The negative signs in Eq. (10) were employed to comply with the nomenclature of Reference 6.*

$$(r\overset{*}{u})_r + \overset{*}{v}_\theta + r\overset{*}{w}_x = 0 \tag{12a}$$

$$\overset{*}{u}_{\bar{t}} + \overset{*}{u}_\theta - 2\overset{*}{v} = -\overset{*}{p}_r + Re^{-1}\,[\nabla^2\overset{*}{u} - r^{-2}\,\overset{*}{u} - 2r^{-2}\,\overset{*}{v}_\theta] \tag{12b}$$

$$\overset{*}{v}_{\bar{t}} + \overset{*}{v}_\theta + 2\overset{*}{u} = -r^{-1}\,\overset{*}{p}_\theta + Re^{-1}\,[\nabla^2\overset{*}{v} - r^{-2}\,\overset{*}{v} + 2r^{-2}\,\overset{*}{u}_\theta] \tag{12c}$$

$$\overset{*}{w}_{\bar{t}} + \overset{*}{w}_\theta = -\overset{*}{p}_x + Re^{-1}\,\nabla^2\overset{*}{w}, \tag{12d}$$

where subscripts denote partial differentiation, $\bar{t} = \overset{*}{\phi}t$, and

$$\nabla^2 \equiv \partial^2/\partial r^2 + r^{-1}\,\partial/\partial r + r^{-2}\,\partial^2/\partial\theta^2 + \partial^2/\partial x^2. \tag{13}$$

The Reynolds number is

$$Re \equiv \overset{*}{\phi}\,a^2/\nu, \tag{14}$$

where ν is the kinematic viscosity of the fluid.

The boundary conditions are: no flow through the bounding walls and no slip along them; i.e.,

$$\hat{u}(\hat{r}=1) = \hat{w}(\hat{r}=1) = 0, \qquad \hat{v}(\hat{r}=1) = 1 \qquad \text{(side)} \tag{15a}$$

$$\hat{u}(\hat{x}=\pm\bar{\bar{c}}) = \hat{w}(\hat{x}=\pm\bar{\bar{c}}) = 0, \qquad \hat{v}(\hat{x}=\pm\bar{\bar{c}}) = \hat{r} \qquad \text{(end)} \tag{15b}$$

where $\hat{u}$, $\hat{v}$, $\hat{w}$ are non-dimensional cylindrical velocity components in the aeroballistic system $\hat{r}$, $\tilde{\theta}$, $\hat{x}$; and $\bar{\bar{c}}$ is the half-height, c, of the cylinder divided by a.

The boundary conditions must be transformed to the coordinates used in Eq. (12); the transformations of Eq. (9) are used to accomplish this.* The resulting non-homogeneous boundary conditions in the inertial system are:

$$\overset{*}{u}_{wall} = (x-\ell)\ \text{Real}\,[-i(1-f)\,\exp\{i(f\overset{*}{\phi}t-\theta)\}] + O(K_o) \tag{16a}$$

$$\overset{*}{v}_{wall} = -(x-\ell)\ \text{Real}\,[(1-f)\,\exp\{i(f\overset{*}{\phi}t-\theta)\}] + O(K_o) \tag{16b}$$

$$\overset{*}{w}_{wall} = -r\ \text{Real}\,[-i(1-f)\,\exp\{i(f\overset{*}{\phi}t-\theta)\}] + O(K_o). \tag{16c}$$

(Recall that $f = (1-i\varepsilon)\tau$.)

---

* *A derivation is outlined in Appendix A.*

The t and θ dependence of the boundary conditions is satisfied by a flow solution of the form

$$\overset{*}{u} = \text{Real } (\overset{*}{u}_C) = \text{Real } [\underset{-}{u}(r,x) \exp \{i(f\overset{*}{\phi}t-\theta)\}] \tag{17a}$$

$$\overset{*}{v} = \text{Real } (\overset{*}{v}_C) = \text{Real } [\underset{-}{v}(r,x) \exp \{i(f\overset{*}{\phi}t-\theta)\}] \tag{17b}$$

$$\overset{*}{w} = \text{Real } (\overset{*}{w}_C) = \text{Real } [\underset{-}{w}(r,x) \exp \{i(f\overset{*}{\phi}t-\theta)\}] \tag{17c}$$

$$\overset{*}{p} = \text{Real } (\overset{*}{p}_C) = \text{Real } [\underset{-}{p}(r,x) \exp \{i(f\overset{*}{\phi}t-\theta)\}], \tag{17d}$$

where $\underset{-}{u}$, $\underset{-}{v}$, $\underset{-}{w}$, and $\underset{-}{p}$ are complex functions. The functions $\overset{*}{u}_C$, $\overset{*}{v}_C$, $\overset{*}{w}_C$, and $\overset{*}{p}_C$ are clearly also solutions of Eq. (12). We substitute these complex solutions into Eq. (12) to obtain:

$$\underset{-r}{ru} + \underset{-}{u} - i\underset{-}{v} + \underset{-x}{rw} = 0 \tag{18a}$$

$$i(f-1)\underset{-}{u} - 2\underset{-}{v} = -\underset{-r}{p} + (1/Re)[\underset{-rr}{u} + \underset{-r}{u}/r - 2\underset{-}{u}/r^2 + \underset{-xx}{u} + 2i\underset{-}{v}/r^2] \tag{18b}$$

$$i(f-1)\underset{-}{v} + 2\underset{-}{u} = i\underset{-}{p}/r + (1/Re)[\underset{-rr}{v} + \underset{-r}{v}/r - 2\underset{-}{v}/r^2 + \underset{-xx}{v} - 2i\underset{-}{u}/r^2] \tag{18c}$$

$$i(f-1)\underset{-}{w} = -\underset{-x}{p} + (1/Re)[\underset{-rr}{w} + \underset{-r}{w}/r - \underset{-}{w}/r^2 + \underset{-xx}{w}]. \tag{18d}$$

The wall boundary conditions of Eq. (16) become

$$\underset{-wall}{u} = -i(1-f)\,(x-\ell), \qquad \underset{-wall}{v} = -(1-f)\,(x-\ell), \tag{19}$$

$$\underset{-wall}{w} = i(1-f)\,r.$$

Axial boundary conditions are

$$\underset{-}{u}(r=0) - i\underset{-}{v}(r=0) = 0, \qquad \underset{-}{w}(r=0) = 0, \tag{20}$$

$$\underset{-}{p}(r=0) = 0.$$

These are required by the equations themselves, assuming that all variables and their derivatives are finite at r=0; a derivation is given in Appendix B.

The solution to Eq. (18) is expressed as the sum of two solutions:

$$\underset{-}{u} = \underset{-p}{u} + \underset{-H}{u}, \qquad \underset{-}{v} = \underset{-p}{v} + \underset{-H}{v} \tag{21}$$

$$\underset{-}{w} = \underset{-p}{w} + \underset{-H}{w}, \qquad \underset{-}{p} = \underset{-p}{p} + \underset{-H}{p},$$

where the particular solution $(\underset{-p}{u}, \underset{-p}{v}, \underset{-p}{w}, \underset{-p}{p})$ is

$$\underset{-p}{u} = -i[(1-f)^2/(1+f)]x + i(1-f)\ell \tag{22a}$$

$$\underset{-p}{v} = -[(1-f)^2/(1+f)]x + (1-f)\ell \tag{22b}$$

$$\underset{-p}{w} = i(1-f)r \tag{22c}$$

$$\underset{-p}{p} = -(1-f)^2 rx + (1-f^2)\,\ell r. \tag{22d}$$

Sidewall boundary conditions are now:

$$\underset{-H}{u}(r=1) = -i[2f(1-f)/(1+f)]x \tag{23a}$$

$$\underset{-H}{v}(r=1) = -[2f(1-f)/(1+f)]x \tag{23b}$$

$$\underset{-H}{w}(r=1) = 0. \tag{23c}$$

Endwall boundary conditions are:

$$\underset{-H}{u}(x=\bar{\bar{c}}) = -i[2f(1-f)/(1+f)]\bar{\bar{c}}, \quad \underset{-H}{u}(x=-\bar{\bar{c}}) = -\underset{-H}{u}(x=\bar{\bar{c}}) \tag{24a}$$

$$\underset{-H}{v}(x=\bar{\bar{c}}) = -[2f(1-f)/(1+f)]\bar{\bar{c}}, \quad \underset{-H}{v}(x=-\bar{\bar{c}}) = -\underset{-H}{v}(x=\bar{\bar{c}}) \tag{24b}$$

$$\underset{-H}{w}(x=\bar{\bar{c}}) = \underset{-H}{w}(x=-\bar{\bar{c}}) = 0. \tag{24c}$$

Axial boundary conditions are the same as those of Eq. (20):

$$\underset{-H}{u}(r=0) - i\underset{-H}{v}(r=0) = \underset{-H}{w}(r=0) = \underset{-H}{p}(r=0) = 0. \tag{25}$$

The total problem is now finally given by Eqs. (18), (23), (24), and (25) for $\underset{-H}{u}$, $\underset{-H}{v}$, $\underset{-H}{w}$, and $\underset{-H}{p}$.

B. Modal Analysis: Separated-Variable Solutions

1. Form of Solution.

The solutions to Eq. (18) will be obtained using separation of variables with the corrected endwall condition described in the next section. This gives rise to a non-standard eigenvalue problem for the x variation. Separation of variables requires solutions of the form

$$\underset{-H}{u}(r,x) = R_1(r)\, X_1(x) \qquad \underset{-H}{w}(r,x) = R_3(r)\, X_3(x) \tag{26}$$

$$\underset{-H}{v}(r,x) = R_2(r)\, X_2(x) \qquad \underset{-H}{p}(r,x) = R_4(r)\, X_4(x)$$

Substituting these into Eq. (18) yields ordinary differential equations for the R's and X's. It can be shown, see Appendix C, that the X_i must satisfy the harmonic equation

$$d^2X_i/dx^2 + \lambda^2 X_i = 0 \tag{27}$$

for i = 1, 2, 3, 4, where λ is the eigenvalue. The equations for R_i are given in Eq. (33) below. The conclusion is that the general form (26) reduces to that assumed in the modal analysis of Reference 5.

Another possible approach is the method of Hall[8], which was developed for circular Couette flow in a finite length cylindrical annulus. It would use a modified form of the theory of Reference 5, and the no-slip condition on the endwall would be satisfied at a finite number of points. One feature of this method, in common with the approach adopted here, is that the λ_k (or k in Reference 5) are complex.

The separation of variables leads to the result that all flow variables have the form

$$R(r)[A_1 \sin \lambda x + A_2 \cos \lambda x].$$

The sidewall boundary conditions Eqs. (23a) and (23b), show that $\underset{-H}{u}$ and $\underset{-H}{v}$ are odd functions of x at r=1; thus series expansions of eigenfunctions should contain only the odd functions; i.e., the sin λx's for $\underset{-H}{u}$ and $\underset{-H}{v}$. Inspection of Eqs. (18a) and (18b) containing these $\underset{-H}{u}$ and $\underset{-H}{v}$ solutions shows that $\underset{-H}{w}$

---

8. *P. J. Blennerhasset and P. Hall, "Centrifugal Instabilities of Circumferential Flow in Finite Cylinders: Linear Theory," Proc. Roy. Soc. London A-365, pp. 191-207, 1979.*

must then contain only cos λx and $\underline{p}_H$ must contain only sin λx. Thus we assume a solution in the form of the following infinite series:*

$$\underline{u}_H = \sum_{k=1} \hat{u}_k(r) \sin \lambda_k x, \qquad \underline{v}_H = \sum_{k=1} \hat{v}(r) \sin \lambda_k x \tag{28}$$

$$\underline{w}_H = -\sum_{k=1} \hat{w}_k(r) \cos \lambda_k x, \qquad \underline{p}_H = \sum_{k=1} \hat{p}_k(r) \sin \lambda_k x.$$

The $\hat{u}_k$, $\hat{v}_k$, $\hat{w}_k$, $\hat{p}_k$ are complex functions which are solutions of Eq. (33) below. In the procedure described next, for satisfying approximately the endwall boundary conditions, Eq. (24), the eigenvalues λ_k are complex; the "uncorrected" form of this boundary condition would give real λ_k and, therefore, the normal modes.

2. Corrected Endwall Boundary Condition

The above solution cannot satisfy all the endwall boundary conditions, Eq. (24). For $\lambda_k = k\pi/(2\bar{\bar{c}})$, where k is odd, it satisfies Eq. (24c) but fails to satisfy the no-slip condition. To correct for this, a procedure analogous to that of Wedemeyer[2,3] is adopted. The technique of matched asymptotic expansions is used to derive the correction; it is explained in detail in Appendix D. The three boundary conditions of Eq. (24) are required to determine the solution to Eq. (18). It is shown in Appendix D that the outer solution to Eq. (18) is determined by only one boundary condition on $\underline{w}_H$. The outer solution is matched to the inner, boundary layer type, solution which satisfies the no-slip condition. The one condition on the outer solution for $\underline{w}_H$ can have different forms for various degrees of approximation. Thus,

$$\underline{w}_H = 0 \quad \text{at } x = \pm \bar{\bar{c}}$$

gives the solution to 0 ($Re^{-1/2}$); this is the uncorrected solution with real λ_k. The next approximation

$$\underline{w}_H - \delta c \, \partial \underline{w}_H/\partial x = 0 \qquad \text{at } x = \bar{\bar{c}} \tag{29a}$$

$$\underline{w}_H + \delta c \, \partial \underline{w}_H/\partial x = 0 \qquad \text{at } x = -\bar{\bar{c}} \tag{29b}$$

gives the solution to 0 (Re^{-1}); this is the corrected solution with complex λ_k.

---

* *The negative sign appears in the $\underline{w}_H$ series for the purpose of facilitating the adaptation of existing programming to the present problem.*

Here non-dimensional δc is given by the following sequence:

$$\alpha = 2^{-1/2}\, Re^{1/2}(1-i)(3-f)^{1/2} \tag{30}$$

$$\beta = 2^{-1/2}\, Re^{1/2}(1+i)(1+f)^{1/2}.$$

$$\delta c = \left[\frac{1}{2\alpha}\left(1 - \frac{2}{1-f}\right) + \frac{1}{2\beta}\left(1 + \frac{2}{1-f}\right)\right].$$

The complex square roots are chosen to be the ones that make the real parts of α and β positive. Detailed expressions are found in Eq. (A.5.) of Reference 5.

The theory giving conditions (29) is asymptotic for $Re \to \infty$. The lower limit on Re that will give a certain accuracy in the solution must be determined by comparison of the results with experiment or by getting the solution using the next term for the boundary conditions to $O(Re^{-3/2})$.

Each $\cos \lambda_k z$ term of $\underset{=}{w}_H$ in Eq. (28) must individually satisfy Eq. (29). Substitution at $x = \pm \underset{=}{c}$ yields the functional equation for the denumerable set of permissible λ_k's,

$$\cos \lambda_k \underset{=}{c} + \lambda_k\, \delta c \sin \lambda_k \underset{=}{c} = 0. \tag{31}$$

For $|\delta c|/\underset{=}{c} \ll 1$,

$$\lambda_k \cong \overset{*}{K} \equiv (k\pi)/[2(\underset{=}{c} - \delta c)] \qquad (\underline{k \text{ odd}}) \tag{32}$$

3. Ordinary Differential Equations for Radial Variation

The solution in Eq. (28) portrays the modal composition of the perturbed flow in the axial direction; each term of the four series is a solution to Eq. (18). When the four k th terms are substituted into Eq. (18), the $\sin \lambda_k x$ and $\cos \lambda_k x$ terms cancel out, leaving the following set of ordinary differential equations for $\hat{u}_k$, $\hat{v}_k$, $\hat{w}_k$, and $\hat{p}_k$ (where $' \equiv d/dr$), omitting subscripts k on the variables:

$$r\hat{u}' + \hat{u} - i\hat{v} + \lambda_k r\hat{w} = 0 \tag{33a}$$

$$Re^{-1}\,\hat{u}'' + (Re\ r)^{-1}\hat{u}' + [i(1-f) - Re^{-1}(2/r^2 + \lambda_k^2)]\hat{u} + \tag{33b}$$

$$[2 + 2i(Re\ r^2)^{-1}]\hat{v} = \hat{p}'$$

$$Re^{-1}\hat{v}'' + (Re\ r)^{-1}\hat{v}' + [i(1-f)-Re^{-1}(2/r^2+\lambda_k^2)]\hat{v} - \tag{33c}$$

$$[2+2i(Re\ r^2)^{-1}]\hat{u} = -i\hat{p}/r$$

$$Re^{-1}\hat{w}'' + (Re\ r)^{-1}\hat{w}' + [i(1-f)-Re^{-1}(1/r^2+\lambda_k^2)]\hat{w} = -\lambda_k\hat{p}. \tag{33d}$$

These equations are converted to canonical form in order to be integrated numerically; i.e.,

$$y_i' \equiv dy_i/dr = f_i(r, y_1, y_2, \ldots y_6), \qquad i = 1, 2, \ldots 6,$$

where

$$\begin{aligned} y_1 &= \hat{u} & y_3 &= \hat{v}' & y_5 &= \hat{w}' \\ y_2 &= \hat{u} - i\hat{v} & y_4 &= \hat{w} & y_6 &= \hat{p}. \end{aligned} \tag{34}$$

After the required manipulations are performed, the following sixth order system is obtained:

$$y_1' = -(y_2/r) - \lambda_k y_4 \tag{35a}$$

$$y_2' = -(y_2/r) - i\ y_3 - \lambda_k y_4 \tag{35b}$$

$$y_3' = 2(Re + i\ r^{-2})y_1 + i(\beta+r^{-2})(y_2-y_1) - y_3/r - i(Re/r)y_6 \tag{35c}$$

$$y_4' = y_5 \tag{35d}$$

$$y_5' = \beta\ y_4 - y_5/r - \lambda_k\ Re\ y_6 \tag{35e}$$

$$y_6' = -Re^{-1}\beta\ y_1 + [2i-(Re\ r^2)^{-1}](y_2-y_1) + i(Re\ r)^{-1}y_3 - \lambda_k\ Re^{-1}y_5 \tag{35f}$$

where

$$\beta \equiv r^{-2} + \lambda_k^2 - i\ Re\ (1-f). \tag{36}$$

4. Boundary Conditions for Radial Equations

There are three boundary conditions at r=0 and three at r=1. As a consequence of Eqs. (25) and (28), conditions at r=0 are (reintroducing the index k) $\hat{u}_k - i\hat{v}_k = \hat{w}_k = \hat{p}_k = 0$, or

$$y_{2k}(0) = y_{4k}(0) = y_{6k}(0) = 0. \tag{37}$$

From Eqs. (23) and (28) we obtain at r = 1:

$$-i[2f(1-f)/(1+f)]\ x = \sum_k \hat{u}_k(1)\ \sin \lambda_k x \tag{38}$$

$$-\ [2f(1-f)/(1+f)]\ x = \sum_k \hat{v}_k(1)\ \sin \lambda_k x$$

$$0 = -\ \sum_k \hat{w}_k(1)\ \cos \lambda_k x.$$

In order to obtain $\hat{u}_k(1)$ and $\hat{v}_k(1)$, we expand the function x in the interval $-\bar{\bar{c}} \leq x \leq \bar{\bar{c}}$ in a series in $X_k(x) \equiv \sin \lambda_k x$:

$$x = \sum_k b_k\ \sin \lambda_k x. \tag{39}$$

The functions $X_k(x)$ are the eigenfunctions of the x-eigenvalue problem discussed in Section III.B.1. When $\delta c = 0$ the λ_k are real and the eigenvalue problem is a standard self-adjoint problem. The eigenfunctions are orthogonal and form a complete set; in fact, the b_k are the Fourier coefficients. For $\delta c \neq 0$, and since δc is complex, a standard self-adjoint problem is not obtained. The eigenfunctions are not orthogonal. They are biorthogonal with respect to the solutions of the <u>adjoint</u> problem, which property enables the b_k to be determined. Some of the details are discussed in Appendix E; here we merely state the coefficients:

$$b_k = \frac{(2/\lambda_k{}^2)\ [1 + (\lambda_k \delta c)^2]\ \sin \lambda_k \bar{\bar{c}}}{\bar{\bar{c}}\ [1 + (\lambda_k\ \delta c)^2] - \delta c} \qquad \underline{(k\ \text{odd})} \tag{40}$$

From Eqs. (34), (38), and (39) the sidewall boundary conditions are:

$$y_{1k}(1) \equiv \hat{u}_k(1) = -i\ [2f(1-f)/(1+f)]\ b_k \tag{41a}$$

$$y_{2k}(1) \equiv \hat{u}_k(1) - i\ \hat{v}_k(1) = 0 \tag{41b}$$

$$y_{4k}(1) \equiv \hat{w}_k(1) = 0. \tag{41c}$$

An alternative set of coefficients, a_k, are also used for the $\sin \lambda_k x$ expansion of x; actually, these had been used before the b_k formula of Eq. (40) was derived. They are determined by optimizing, in a least squares sense, the fit

of the partial sum, $\sum_{k=1}^{kf} a_k \sin \lambda_k x$ (k odd), to the function x over the interval $-\bar{\bar{c}} \leq x \leq \bar{\bar{c}}$. Thus, the (kf-1)/2 a_k's are calculated which minimize the following integral (where k is odd):

$$I(a_1, a_3, \ldots a_{kf}) \equiv \int_{-\bar{\bar{c}}}^{\bar{\bar{c}}} \left| x - \sum_{k=1}^{kf} a_k \sin \lambda_k x \right|^2 dx. \qquad (42)$$

In our work the minimization was carried out with a preprogrammed computer routine that involved an iterative operation. The Fourier series,

$$x = \sum_{k=1} \left[(-1)^{(k-1)/2} \, 8\bar{\bar{c}}/(\pi k)^2 \right] \sin \left[k\pi/(2\bar{\bar{c}}) \right] x \qquad (k \text{ odd}),$$

furnished good initial guesses for the a_k's. We have generally used eight terms in the series of Eq. (39) or its counterpart with a_k's. These have furnished sufficiently accurate representations of the function x.

5. Numerical Procedures.

The differential system, Eq. (35), and initial conditions, Eq. (37), constitute the same numerical integration problem, including orthonormalization, as does the eigenfrequency determination[5]. We refer the reader to Reference 5 for a detailed description of the numerical procedures. One difference arises because the terminal conditions, Eq. (41), are non-homogeneous.

In the orthonormalization process[5], the interval $0 \leq r \leq 1$ is divided into N sub-intervals. In each subinterval three linearly independent solutions for $\hat{u}$, $\hat{v}$, $\hat{w}$, $\hat{p}$ which originally satisfy the initial conditions at r = 0 are found, and these are combined linearly so that the total solution is continuous at the boundaries of the sub-intervals. The process of determining the coefficients of the combinations begins in the last (N th) subinterval by applying the inhomogeneous sidewall conditions at r = 1 for a given k:

$$\begin{aligned}
c_{1N} \hat{u}_{1N}(1) + c_{2N} \hat{u}_{2N}(1) + c_{3N} \hat{u}_{3N}(1) &= \hat{u}(1) \\
c_{1N} \hat{v}_{1N}(1) + c_{2N} \hat{v}_{2N}(1) + c_{3N} \hat{v}_{3N}(1) &= \hat{v}(1) \qquad (43) \\
c_{1N} \hat{w}_{1N}(1) + c_{2N} \hat{w}_{2N}(1) + c_{3N} \hat{w}_{3N}(1) &= 0.
\end{aligned}$$

The quantities on the right-hand sides are obtained from Eq. (41). The other sets of c_1, c_2, c_3 for the succeeding subintervals can now be determined in sequence proceeding from r = 1 to r = 0 by the method described in Section III.E. of Reference 5.

IV. EVALUATION OF PRESSURE

The flow variable of primary interest here is the pressure. From Eq. (17d),

$$\overset{*}{p} = e^{\varepsilon\dot{\phi}\tau t}\left[-\underset{\sim}{p}_I \sin(\tau\dot{\phi}t - \theta) + \underset{\sim}{p}_R \cos(\tau\dot{\phi}t - \theta)\right] + O(K_0), \tag{44}$$

where

$$\underset{\sim}{p}(r,x) = \underset{\sim}{p}_R + i\,\underset{\sim}{p}_I. \tag{45}$$

The total pressure, to within an additive constant, recalling Eqs. (10) and (11), is

$$p = \frac{1}{2}r^2 - K_0\overset{*}{p}. \tag{46}$$

The liquid moment calculations call for pressure evaluations at constant values of $\tilde{r}$ and $\tilde{x}$. Accordingly, the $\frac{1}{2}r^2$ term in Eq. (46) is replaced, from Eq. (9a), by

$$\frac{1}{2}r^2 = \frac{1}{2}\tilde{r}^2 - K_0\, e^{\varepsilon\dot{\phi}\tau t}\, r(x-\ell)\cos(\tau\dot{\phi}t - \theta) + O(K_0^2). \tag{47}$$

Thus, by Eqs. (46) and (47), the disturbance pressure, which is measured at points fixed on the cylinder surface, is

$$Dp \equiv p - \frac{1}{2}\tilde{r}^2 = \frac{1}{2}r^2 - \frac{1}{2}\tilde{r}^2 - K_0\overset{*}{p}.$$

$$Dp \equiv p - \frac{1}{2}\tilde{r}^2 = -K_0\, e^{\varepsilon\tau\dot{\phi}t}\left[-\underset{\sim}{p}_I \sin(\tau\dot{\phi}t - \theta) + \right.$$

$$\left. + \{\underset{\sim}{p}_R + r(x-\ell)\}\cos(\tau\dot{\phi}t - \theta)\right]. \tag{48}$$

The r, θ, x in the bracketed term of Eq. (48) can be replaced by $\tilde{r}$, $\tilde{\theta}$, $\tilde{x}$ without changing the order of the approximation since $\tilde{r} = r + 0\ (K_0)$, $\tilde{\theta} = \theta + 0\ (K_0)$, $\tilde{x} = x + 0\ (K_0)$. Hence, $Dp\ (\tilde{r} = 1) = Dp\ (r=1) + 0\ (K_0^2)$ and $Dp\ (\tilde{x} = \pm \tilde{c}) = Dp\ (x = \pm \tilde{c}) + 0\ (K_0^2)$. By Eqs. (21), (22d), and (28),

$$\underset{-R}{p} = \text{Real}\left[\sum_k \hat{p}_k(r) \sin \lambda_k x + (1-f^2)\, \ell\, r - (1-f)^2\, r\, x\right] \tag{49}$$

$$\underset{-I}{p} = \text{Imag}\left[\sum_k \hat{p}_k(r) \sin \lambda_k x + (1-f^2)\, \ell\, r - (1-f)^2\, r\, x\right].$$

The disturbance pressure of Eq. (48) is rewritten as

$$Dp = -K_0 e^{\varepsilon\tau\dot{\phi}t}\left[P_1 \sin(\phi_1 - \theta) + P_2 \cos(\phi_1 - \theta)\right] \tag{50}$$

where $P_1 = -\underset{-I}{p}$, $P_2 = \underset{-R}{p} + r\,(x-\ell)$.

Amplitude and phase of Dp are denoted, respectively, by

$$C_p = (P_1^2 + P_2^2)^{1/2} \quad \text{and} \quad \psi = \tan^{-1}(P_2/P_1), \tag{51}$$

so that $Dp = -K_0 e^{\varepsilon\tau\dot{\phi}t}\, C_p \sin\left[(\phi_1-\theta) + \psi\right]$.

The pressure measurements of Whiting[9] can be compared with our pressure calculations. In these experiments the liquid is first completely spun up in an unyawed cylinder; then the cylinder is nutated at a fixed small angle of yaw about its center ($\ell = 0$) with a fixed frequency. Built-in pressure-measuring apparatus enables the disturbance pressure to be measured at two points on the endwall. For comparison we choose data from Figures 10a, 10c, 10d, 10e in Reference 9, which show C_p measurements plotted against the forced coning frequency, τ.

The comparison is shown in Figures 2 and 3. The solid curves are plots of the present computations of C_p. The locations of the peaks, in the experimental data and theoretical results, agree to within about 2.5%. The largest discrepancies in amplitude in Figures 2a and 3a occur at the peaks, where the differences are approximately 15%. The overall percentagewise agreement is poorest in Figure 2b, where the Reynolds number is two orders of magnitude

---

9. *R. D. Whiting, "An Experimental Study of Forced Asymmetric Oscillations in a Rotating Liquid-Filled Cylinder," BRL Technical Report ARBRL-TR-02376, October 1981. AD A107948.*

smaller than those of the other cases. It was noted above that the error in the theory increases as Re decreases; this may be reflected in Figure 2b. We note that the percentagewise scatter in the measurements is also greatest for this case.

Computations by the theory of Reference 6 are also plotted. In Figures 2a, 3a, and 3b they are indistinguishable from the solid line curves. In the low Reynolds number case, however, the differences are significant and the results of Reference 6 show better agreement with measurement. The eigenfrequency, C_R, computed by the method of Reference 5, is indicated for each case in Figures 2 and 3 and in all subsequent figures. In diagrams having peaks, namely those for pressure coefficient, side moment coefficient, and yaw growth rate, it is seen that the τ-value at the peak is very close to C_R for large Reynolds numbers, but that the difference between these two frequencies increases as Reynolds number decreases.

V. LIQUID PRESSURE MOMENTS

Our objective is to determine the moment produced by the liquid on the spinning and nutating shell, namely, $M_{L\tilde{Y}} + i\, M_{L\tilde{Z}}$ of Eq. (5). We shall evaluate the moment about the center of gravity of the projectile in the $\tilde{x}$, $\tilde{y}$, $\tilde{z}$ system. Details need be shown for only one component, say $M_{L\tilde{Z}}$, because of axisymmetry in the transverse motion.

$$M_{L\tilde{Z}} = M_{L\tilde{Z}S} + M_{L\tilde{Z}T} + M_{L\tilde{Z}B} \tag{52}$$

The three terms on the right-hand side denote the moments on the side, top, and bottom walls, respectively.*

$$M_{L\tilde{Z}S} = (\rho a^5 \dot{\phi}^2)\left[\int_{-\bar{c}}^{\bar{c}} \int_0^{2\pi} p\ (\tilde{r}=1)\ (\tilde{x}-\ell)\cos\tilde{\theta}\, d\tilde{\theta}\, d\tilde{x}\right] \tag{53a}$$

$$M_{L\tilde{Z}T} = -(\rho a^5 \dot{\phi}^2)\left[\int_0^1 \int_0^{2\pi} p\ (\tilde{x}=\bar{c})\ \tilde{r}^2 \cos\tilde{\theta}\, d\tilde{\theta}\ \ d\tilde{r}\right] \tag{53b}$$

$$M_{L\tilde{Z}B} = (\rho a^5 \dot{\phi}^2)\left[\int_0^1 \int_0^{2\pi} p\ \ (\tilde{x}=-\bar{c})\ \tilde{r}^2 \cos\tilde{\theta}\, d\tilde{\theta}\ \ d\tilde{r}\ \right] \tag{53c}$$

**Formulas for $M_{L\tilde{Z}S}$, $M_{L\tilde{Z}T}$, and $M_{L\tilde{Z}B}$ are found in Section 3-3.1 of Reference 7. Eqs. (3-31) and (3-30a) contain errors in sign; there should be negative signs before the integrals.*

The non-dimensional cylinder radius occurring in the integrand of Eq. (53a) is equal to 1.

When p, of Eq. (48), is substituted into Eq. (53), the $1/2\ \tilde{r}^2$ term makes no contribution to the integrals, and the lowest order terms therefore are $O(K_o)$. Hence for first order accuracy in K_o the integrands may be evaluated in the earth-fixed system. The integrals become:

$$M_{L\tilde{Z}S}/(\rho a^5 \dot{\phi}^2) = -\pi K_1 \left[(\sin \phi_1) \int_{-\bar{c}}^{\bar{c}} -(x-\ell)\ \underline{p}_I(r=1)\ dx + (\cos \phi_1) \int_{-\bar{c}}^{\bar{c}} (x-\ell) \left\{ \underline{p}_R\ (r=1) + (x-\ell) \right\} dx \right] \tag{54a}$$

$$M_{L\tilde{Z}T}/(\rho a^5 \dot{\phi}^2) = \pi K_1 \left[(\sin \phi_1) \int_0^1 -r^2\ \underline{p}_I\ (x=\bar{c})\ dr + (\cos \phi_1) \int_0^1 r^2 \left\{ \underline{p}_R\ (x=\bar{c}) + r\ (\bar{c}-\ell) \right\} dr \right] \tag{54b}$$

$$M_{L\tilde{Z}B}/(\rho a^5 \dot{\phi}^2) = -\pi K_1 \left[(\sin \phi_1) \int_0^1 -r^2\ \underline{p}_I\ (x=-\bar{c})\ dr + (\cos \phi_1) \int_0^1 r^2 \left\{ \underline{p}_R\ (x=-\bar{c}) - r\ (\bar{c}+\ell) \right\} dr \right]. \tag{54c}$$

The net moment on the endwalls is

$$M_{L\tilde{Z}E} = M_{L\tilde{Z}T} + M_{L\tilde{Z}B}.$$

$$M_{L\tilde{Z}E}/(\rho a^5 \dot{\phi}^2) = \pi K_1 \left[\sin \phi_1 \int_0^1 -r^2 \left\{ \underline{p}_I\ (x=\bar{c}) - \underline{p}_I\ (x=-\bar{c}) \right\} dr + \cos \phi_1 \int_0^1 r^2 \left\{ \underline{p}_R\ (x=\bar{c}) - \underline{p}_R\ (x=-\bar{c}) + 2\ rc \right\} dr \right]. \tag{55}$$

We observe that $M_{L\tilde{Z}E}$ is independent of ℓ.

The moments of Eqs. (54a) and (55) have the form:

$$M_{L\tilde{Z}S} = - K_1 (M_{1S} \sin \phi_1 + M_{2S} \cos \phi_1) (\rho a^5 \dot{\phi}^2) \tag{56}$$

$$M_{L\tilde{Z}E} = - K_1 (M_{1E} \sin \phi_1 + M_{2E} \cos \phi_1) (\rho a^5 \dot{\phi}^2).$$

The moment coefficients M_{1S}, M_{2S}, M_{1E}, and M_{2E} are functions of Re, c/a, τ, and ε.

$$M_{1S} = - \pi \, \text{Imag} \left[\int_{-\bar{c}}^{\bar{c}} (x-\ell) \, \underline{p} \, (r=1) \, dx \right] \tag{57a}$$

$$M_{2S} = \pi \, \text{Real} \left[\int_{-\bar{c}}^{\bar{c}} (x-\ell) \, \underline{p} \, (r=1) \, dx + (2/3) \, (\bar{c}^3 + 3 \, \bar{c}\ell^2) \right] \tag{57b}$$

$$M_{1E} = \pi \, \text{Imag} \left[\int_0^1 r^2 \left\{ \underline{p} \, (x=\bar{c}) - \underline{p} \, (x=-\bar{c}) \right\} dr + c/2 \right] \tag{57c}$$

$$M_{2E} = - \pi \, \text{Real} \left[\int_0^1 r^2 \left\{ \underline{p} \, (x=\bar{c}) - \underline{p} \, (x=-\bar{c}) \right\} dr + c/2 \right]. \tag{57d}$$

The total moment is:

$$M_{L\tilde{Z}} = M_{L\tilde{Z}S} + M_{L\tilde{Z}E} = -K_1 (\rho a^5 \dot{\phi}^2) (M_1 \sin \phi_1 + M_2 \cos \phi_1), \tag{58}$$

where $M_1 = M_{1S} + M_{1E}$, $M_2 = M_{2S} + M_{2E}$. (59)

Our computational results will be exhibited in terms of the moment coefficient, C_{LM}, defined in Eqs. (5) and (6). By Eqs. (5), (6), and (58),

$$C_{LSM} = -M_2 / [2\pi\tau c/a], \qquad C_{LIM} = -M_1 / [2\pi\tau c/a]. \tag{60}$$

Computations of C_{LSM} and C_{LIM} were performed for four Reynolds numbers covering several orders of magnitude: Re = 1×10^3, 5×10^3, 5×10^4, and 5×10^5. Two aspect ratios, 3.126 and 1.042, were employed, pertinent to apparatus currently available for experiments. A single value of ε was considered, namely $\varepsilon = 0.02$, which lies in the region of maximum yaw growth rate occurring in BRL gyroscope experiments; and, finally, $\ell = 0$.

Our interest lies primarily in the side-plane moment, which is the component that affects the yaw of the projectile. Figures 4 and 5 show plots of C_{LSM} versus nutational frequency, τ. The decrease of amplitude and flattening of peak with decreasing Reynolds number is clearly evident for both aspect ratios. Switching the aspect ratio from 3.126 to 1.042 changes the natural mode primarily being excited by the same range of forcing frequencies, and the new amplitudes consequently differ appreciably from the old.

For comparison of our output with other results we look at computations by the Reference 6 method (pressure moments only) for the same cases. Corresponding curves lie very close together for Re = 5×10^4 and 5×10^5 for both aspect ratios, and divergence increases as Reynolds number decreases. Generally, the Reference 6 method gives higher peaks than the present method.

Additional comparisons are made for the C_{LIM}, the in-plane moment coefficient, in Figures 6 and 7. Again, the agreement varies in an inverse manner with Reynolds number.

VI. YAW GROWTH RATE

If the forcing moment of Eq. (2) has the form

$$M_{LY}\hat{Y} + i\, M_{LZ}\hat{Z} = \text{const} \times \hat{\xi},$$

then the following expression is a solution to Eq. (2):

$$\hat{\xi} = K_0 e^{\varepsilon\tau\dot{\phi}t}\, e^{i\tau\dot{\phi}t} = K_0 e^{if\dot{\phi}t}. \tag{61}$$

This is exactly the motion assumed in Eq. (3) for the purpose of calculating the liquid moment. The amplitude variation is governed by the yaw growth rate, $\varepsilon\tau\dot{\phi}$. The growth rate factor, ε, gives a measure of the yaw growth or decay in one nutational cycle. If $\varepsilon>0$, $|\hat{\xi}|$ grows until the small yaw assumption is no longer valid.

Eq. (61) is a solution to Eq. (2) only for a restricted set of f's; these values are the solutions to the functional equation obtained by substituting Eq. (61) into Eq. (2):

$$I_y f^2 - I_x f - I_y \hat{M}/\dot{\phi}^2 = \rho a^5 F(f), \tag{62}$$

where F is also a function of the properties of the fluid, the dimensions of the cavity, and the spin-rate.

According to Stewartson-Wedemeyer, F of Eq. (62) is negligibly small except near resonance. A resonance condition will generally occur when $\tau_n \approx C_R$, where $\tau_n \dot{\phi}$ is the nutational frequency of the empty shell and C_R is a natural inertial frequency of the rotating liquid.

$$\tau_n = \left[I_x + (I_x^2 + 4\, I_y\, \hat{M}/\dot{\phi}^2)^{1/2} \right] \Big/ (2\, I_y).$$

For $\tau \approx C_R$, F can be approximated by the first term of the Laurent series of a function with a simple pole[1,3]

$$F \cong D \,/\, (f - C_R),$$

where the residue, D, depends on the parameters of the problem. In this case Eq. (62) yields three complex solutions for f. Only those solutions are applicable for which $\tau \approx C_R$; generally one of these will have a positive ε. Experiments have consistently shown that for a significant span of time, the motion is described by an exponential solution with positive ε.

In our analysis, applicable also away from resonance, the $\tilde{\xi}$ of Eq. (61) and the moment of Eq. (5) are substituted into Eq. (2) to yield the following functional equation for f:

$$I_y\, f^2 - I_x\, f - I_y\, \hat{M}/\dot{\phi}^2 = -i(2\pi\, \rho a^4 c)\, \tau\, C_{LM}\,(f;\, Re,\, c/a). \qquad (63)$$

This equation must be solved by iteration; outputs from the Stewartson-Wedemeyer theory furnish guidelines for choosing initial estimates of f.

The motion parameter f ($\equiv \tau - i\varepsilon\tau$), has been measured in gyroscope experiments*. The calculations of Murphy[6] indicate that viscous shear contributes significantly to the liquid moment and should not be omitted. Since our pressure moment calculations constitute results of incomplete theory, we

---

* *Applicability of gyroscope experiments to simulation of projectile angular motion is discussed in Section 2-7 of Reference 7.*

shall not make any systematic comparison with data from gyroscope experiments. However, we do demonstrate in Figure 8 the capability of our program to produce yaw growth rate. We choose two cases; the first was treated in Figure 8 of Reference 4, and the second is one of six based on measurements described in Reference 10. The six above-mentioned cases are low Reynolds number experiments, and the only one with $Re>10^4$ is shown in Figure 8.

The parameter that is varied is $\tau_n = I_x/I_y$ (since $\hat{M} = 0$); in the first cases I_y is held constant, and in the second case I_x is held constant. The quantities τ and ε are measured simultaneously; data are presented in the form of $\varepsilon\tau$ vs τ plots. Values of τ_n are chosen that lie close to first radial mode eigenfrequencies of the liquid, namely, $k = 3$ for $c/a = 3.15$, and $k = 1$ for $c/a = 1.04$.

Also shown in Figure 8 are yaw growth rates predicted by the Stewartson-Wedemeyer theory, which likewise treats only the pressure moment. The complex f is computed from the cubic equation described in the discussion following Eq. (63). The pairs of theoretical curves agree very well for $Re = 5.2 \times 10^5$ but differ significantly for the $Re = 1.24 \times 10^4$ case. For both theories the peaks lie to the left of the experimental peaks.

VII. DISCUSSION

We have presented a detailed treatment of the linearized problem of flow of a liquid in a filled spinning cylinder executing angular motion at small yaw, and we have exhibited the consequent moments exerted by the liquid on the cylinder walls. The angular motion takes the form of nutation at constant frequency about an axial point, and yaw growth at an exponential rate; the liquid is in solid-body rotation before the angular motion begins. This motion approximates the actual motion of the liquid-filled projectile over a significant span of its flight history.

The emphasis of this report is directed primarily to the method of determining output rather than to the output itself, which can be treated in more detail in later studies. We feel it worthwhile to include details of equations, formulas, assumptions, and derivations involved in the lengthy computations required to attain the liquid pressure and moment results.

The agreement of our results with those from the concurrent work of Murphy[6], who extended the Stewartson-Wedemeyer theory, tends to support the conclusions from both; the basic assumptions of linearity and solid body are common to both approaches. In addition, both make use of boundary condition corrections which are applicable for large Reynolds numbers.

Future theoretical work will include the additional calculation of viscous shear moments. Experimental work at high Reynolds numbers will also have to be performed in order to provide an adequate data base for validating the theory.

---

10. *W. P. D'Amico, Jr., and T. H. Rogers, "Yaw Instabilities Produced by Rapidly Rotating, Highly Viscous Liquids," AIAA Paper AIAA-81-0224, AIAA 19th Aerospace Sciences Meeting, St. Louis, Missouri, January 12-15, 1981.*

VIII. ACKNOWLEDGEMENT

The authors express their appreciation to Mr. James Bradley for supplying the data of the Murphy theory for the figures of this report.

REFERENCES

1. K. Stewartson, "On the Stability of a Spinning Top Containing Liquid," J. Fluid Mech., Vol. 5, Part 4, September 1959, pp. 577-592.

2. E. H. Wedemeyer, "Dynamics of Liquid-Filled Shell: Theory of Viscous Corrections to Stewartson's Stability Problem," BRL Report 1287, June 1965. AD 472474.

3. E. H. Wedemeyer, "Viscous Corrections to Stewartson's Stability Criterion," BRL Report 1325, June 1966. AD 489687.

4. R. Whiting and N. Gerber, "Dynamics of a Liquid-Filled Gyroscope: Update of Theory and Experiment," BRL Technical Report ARBRL-TR-02221, March 1980. AD A083886.

5. C. W. Kitchens, Jr., N. Gerber, and R. Sedney, "Oscillations of a Liquid in a Rotating Cylinder: Part I. Solid-Body Rotation," BRL Technical Report ARBRL-TR-02081, June 1978. AD A057759.

6. C. H. Murphy, "Angular Motion of a Spinning Projectile with a Viscous Liquid Payload," BRL Technical Report in preparation.

7. Engineering Design Handbook, Liquid-Filled Projectile Design, AMC Pamphlet 706-165, April 1969. AD 853719.

8. P. J. Blennerhasset and P. Hall, "Centrifugal Instabilities of Circumferential Flow in Finite Cylinders: Linear Theory," Proc. Roy. Soc. London A-365, pp. 191-207, 1979.

9. R. D. Whiting, "An Experimental Study of Forced Asymmetric Oscillations in a Rotating Liquid-Filled Cylinder," BRL Technical Report ARBRL-TR-02376, October 1981. AD A107948.

10. W. P. D'Amico, Jr., and T. H. Rogers, "Yaw Instabilities Produced by Rapidly Rotating, Highly Viscous Liquids," AIAA Paper 81-0224, AIAA 19th Aerospace Sciences Meeting, St. Louis, Missouri, 12-15 January 1981.

11. M. Van Dyke, Perturbation Methods in Fluid Mechanics, Academic Press, New York, NY, 1964.

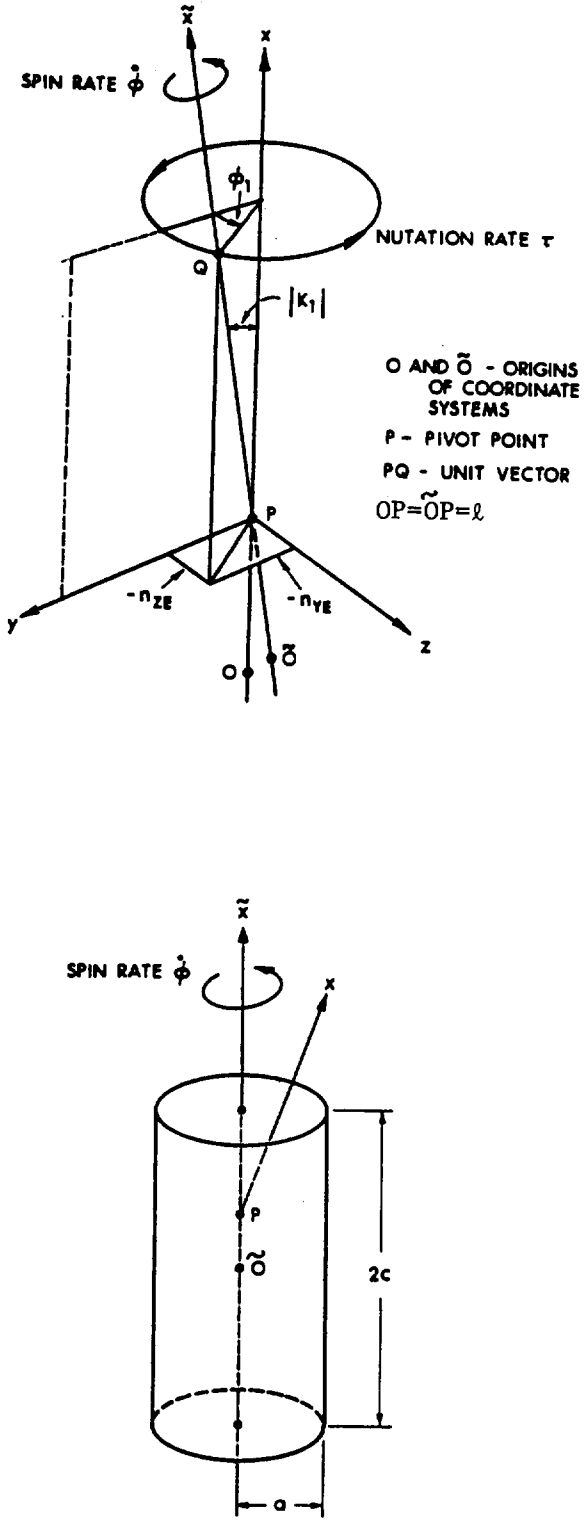

Figure 1. Diagrams of Coordinates and Cylinder.

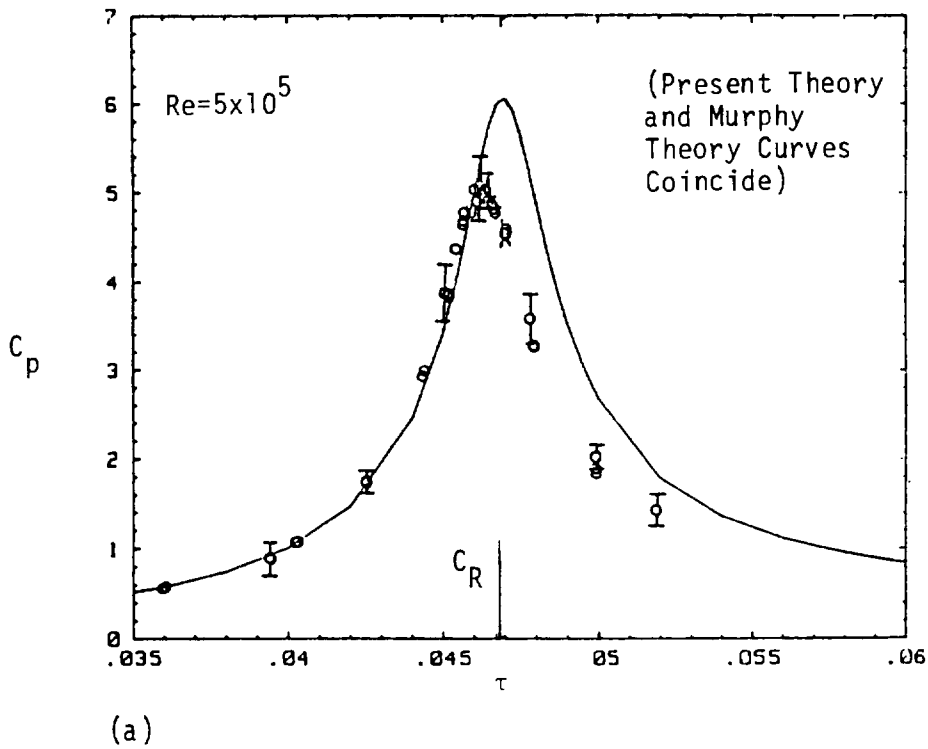

(a)

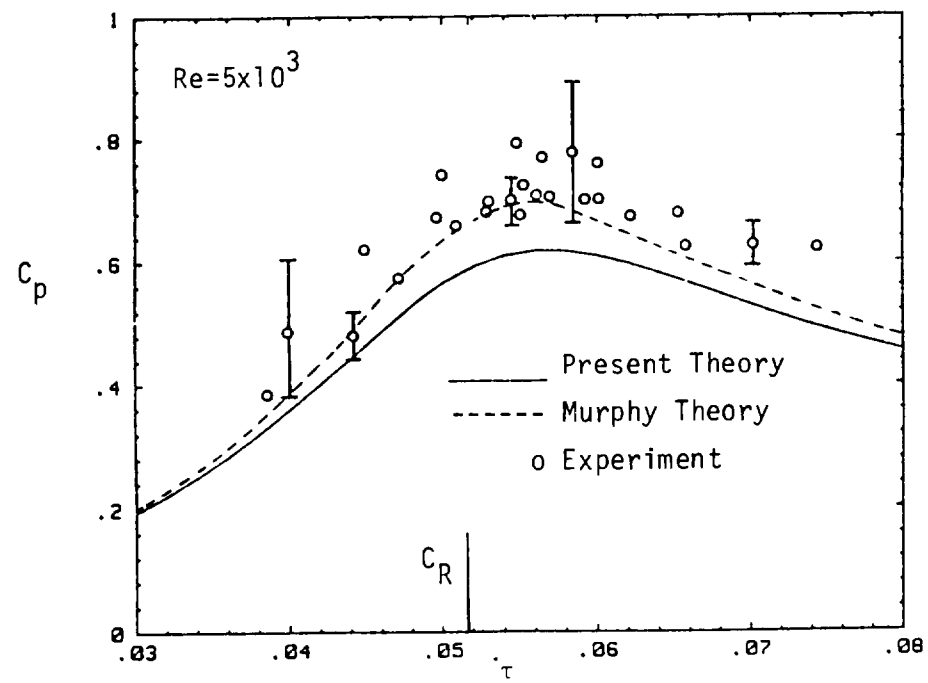

(b)

Figure 2. Comparison of Theoretical and Experimental Endwall Pressure Coefficients (r=0.67, c/a=3.148, ε=0.0).

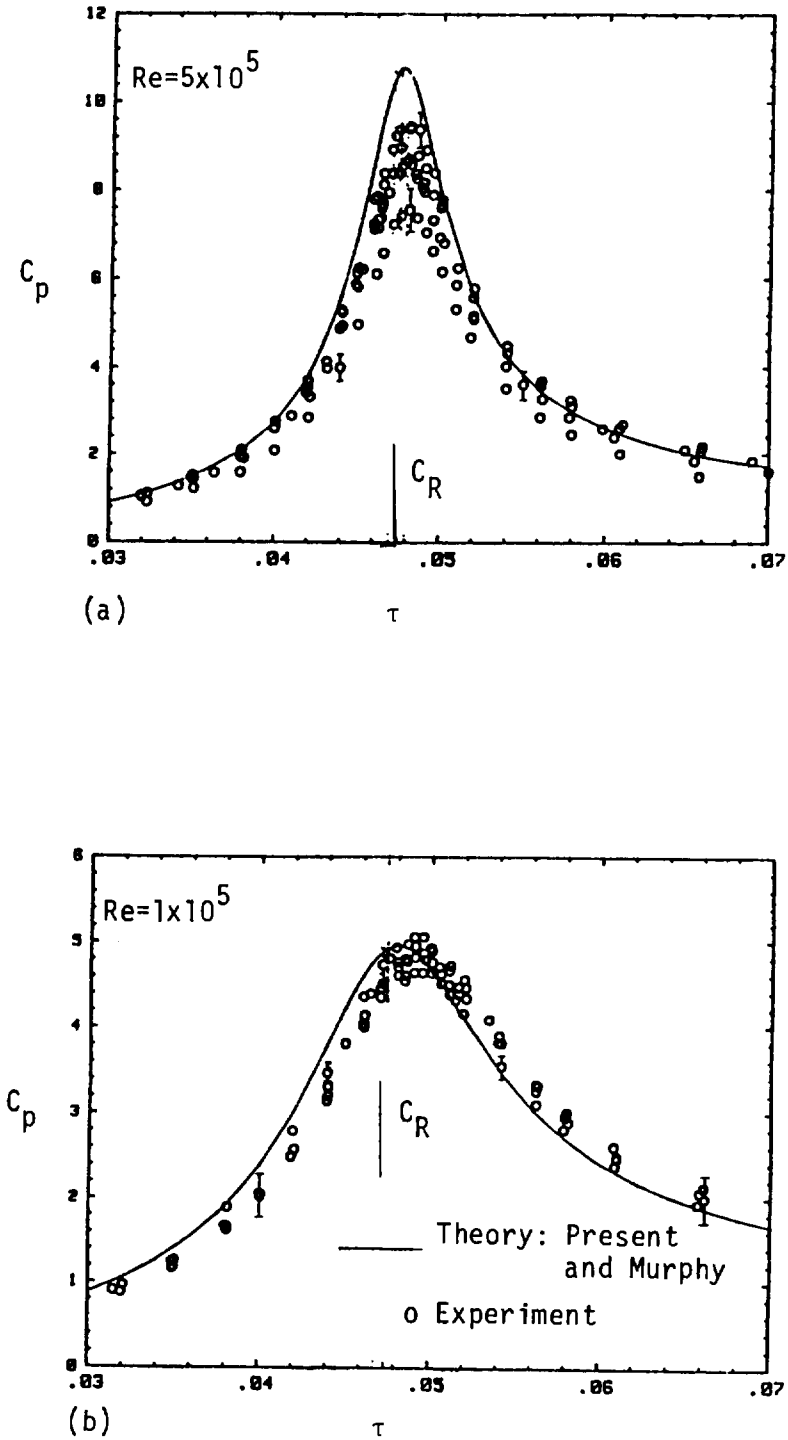

Figure 3. Comparison of Theoretical and Experimental Endwall Pressure Coefficients ($r=0.67$, $c/a=1.051$, $\varepsilon=0.0$).

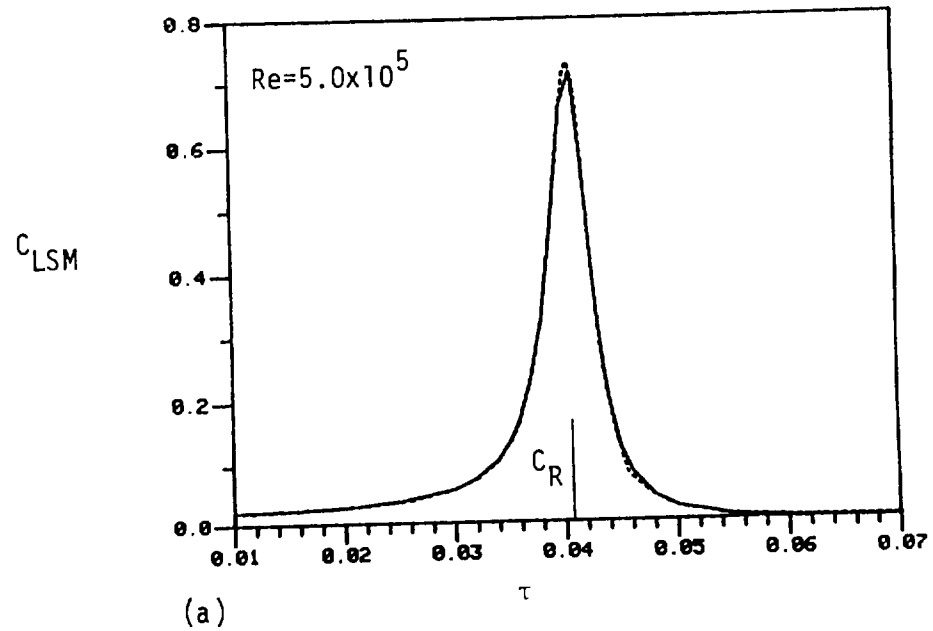

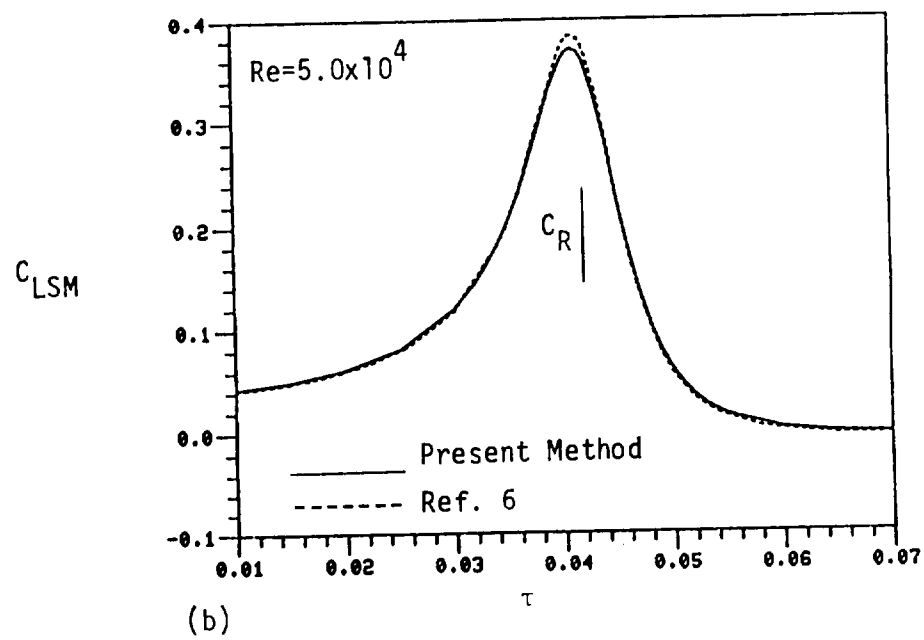

Figure 4. Side Moment Coefficient: Comparison of Results of Present Method and Method of Reference 6 (c/a=3.126, ε=0.02).

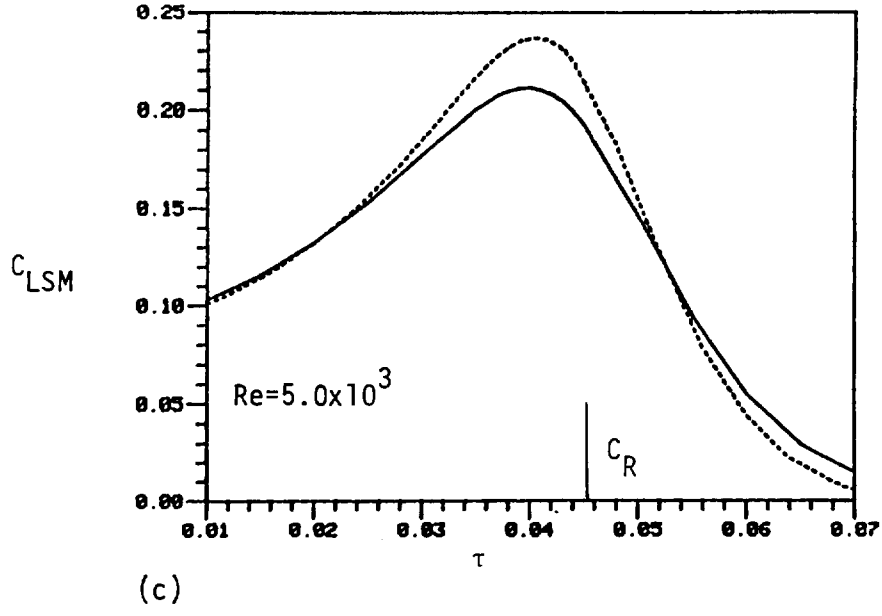

(c)

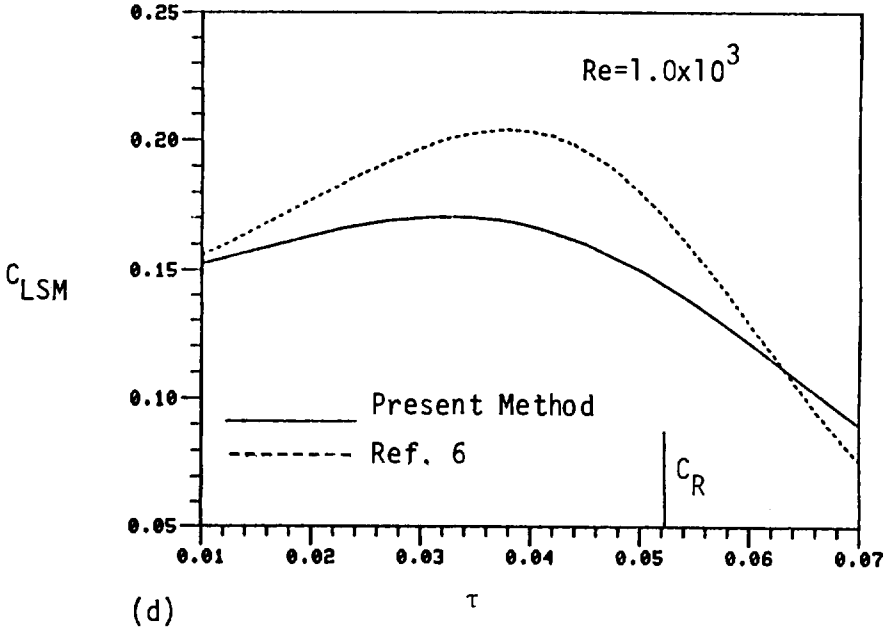

(d)

Figure 4. Side Moment Coefficient: Comparison of Results of Present Method and Method of Reference 6(c/a=3.126, ε=0.02 (cont.).

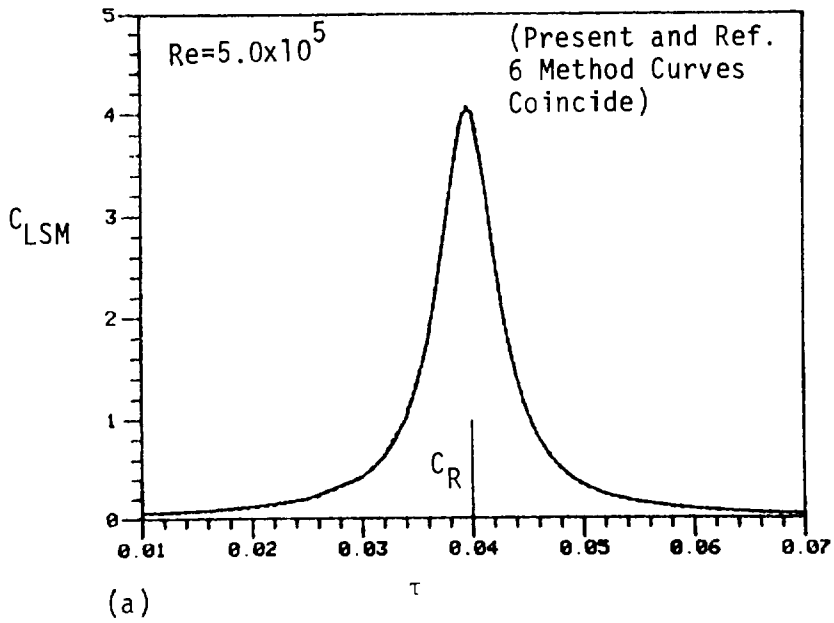

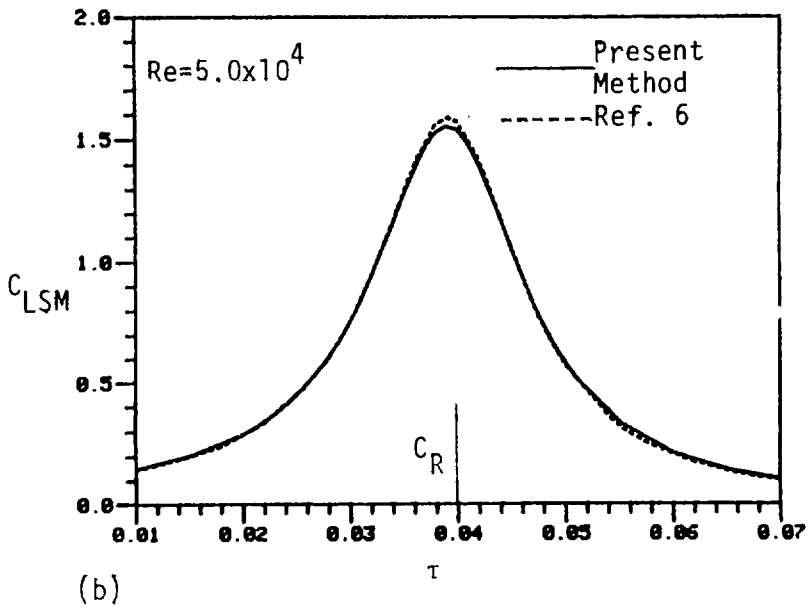

Figure 5. Side Moment Coefficient: Comparison of Results of Present Method and Method of Reference 6 (c/a=1.042, ε=0.02).

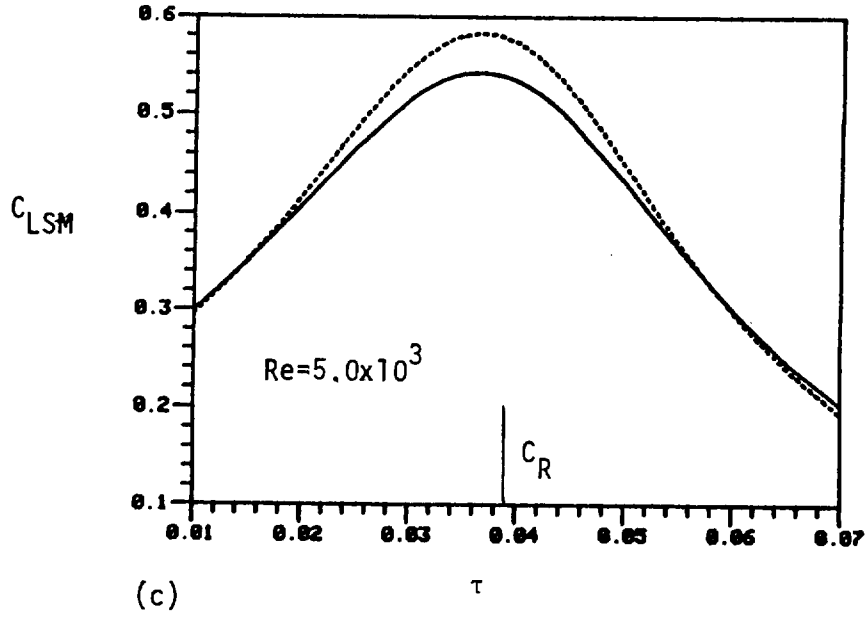

(c)

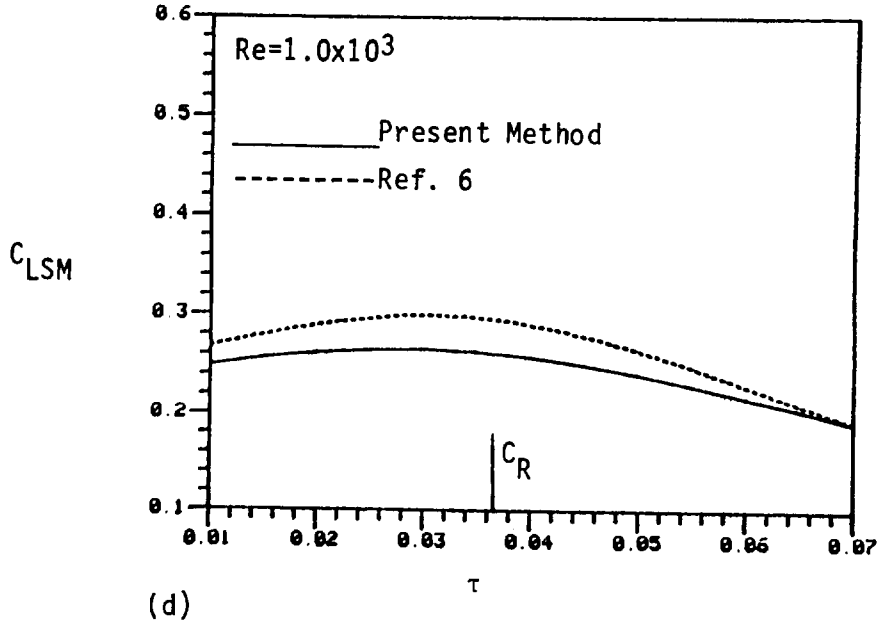

(d)

Figure 5. Side Moment Coefficient: Comparison of Results of Present Method and Method of Reference 6 (c/a=1.042, ϵ=0.02) (cont.).

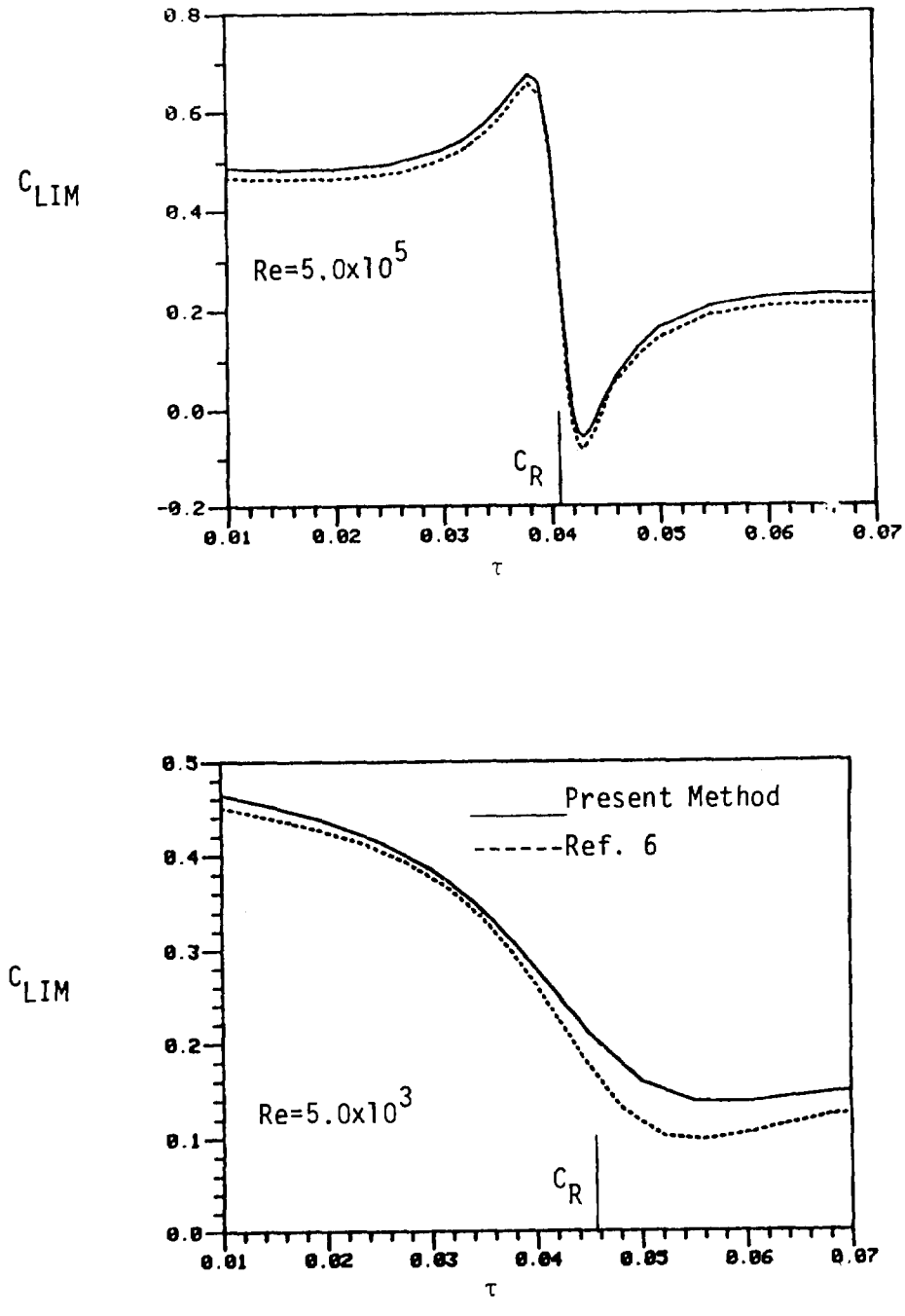

Figure 6. In-Plane Moment Coefficient: Comparison of Results of Present Method and Method of Reference 6 (c/a=3.126, ε=0.02).

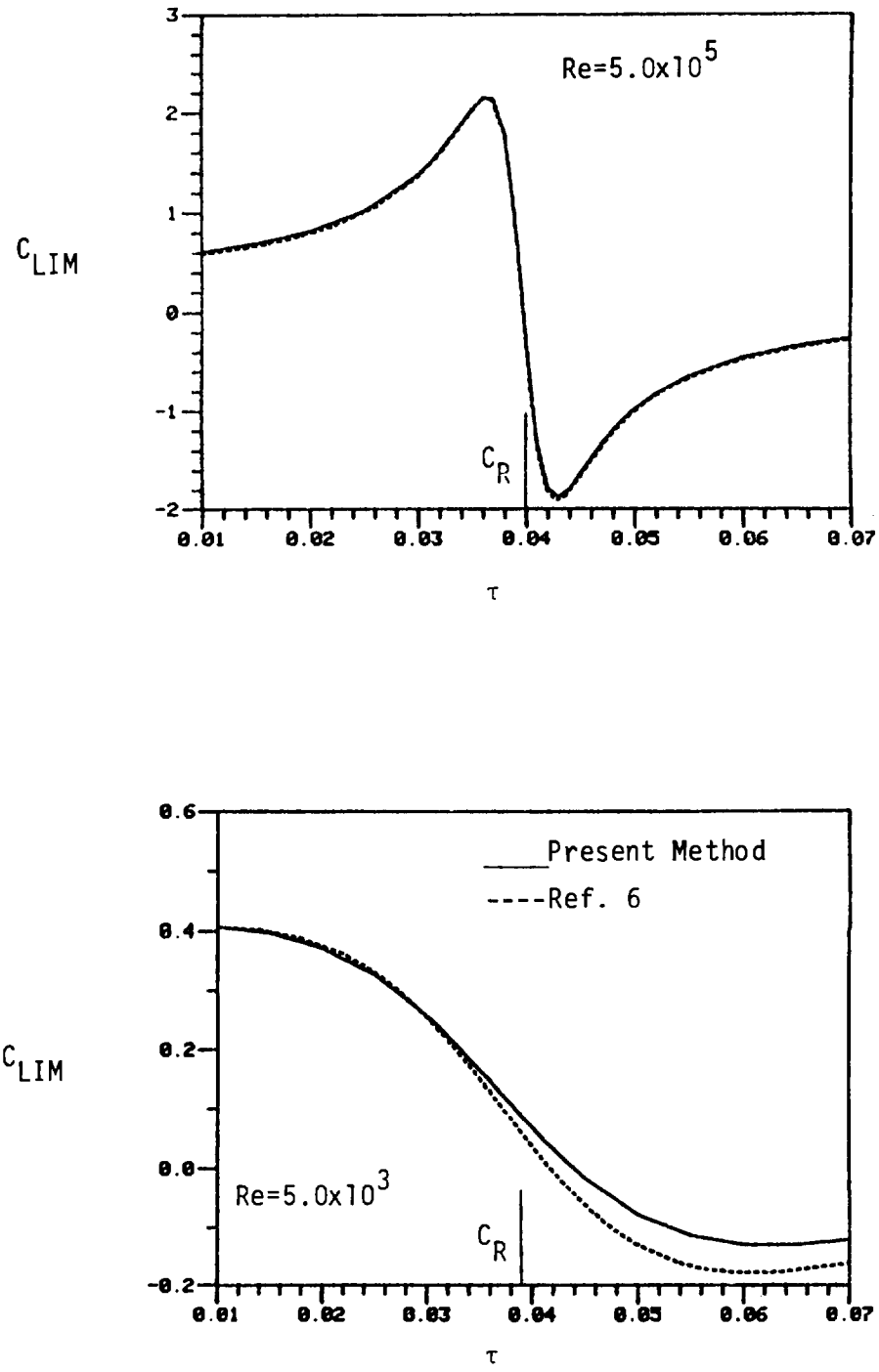

Figure 7. In-Plane Moment Coefficient: Comparison of Results of Present Method and Method of Reference 6 (c/a=1.042, ε=0.02).

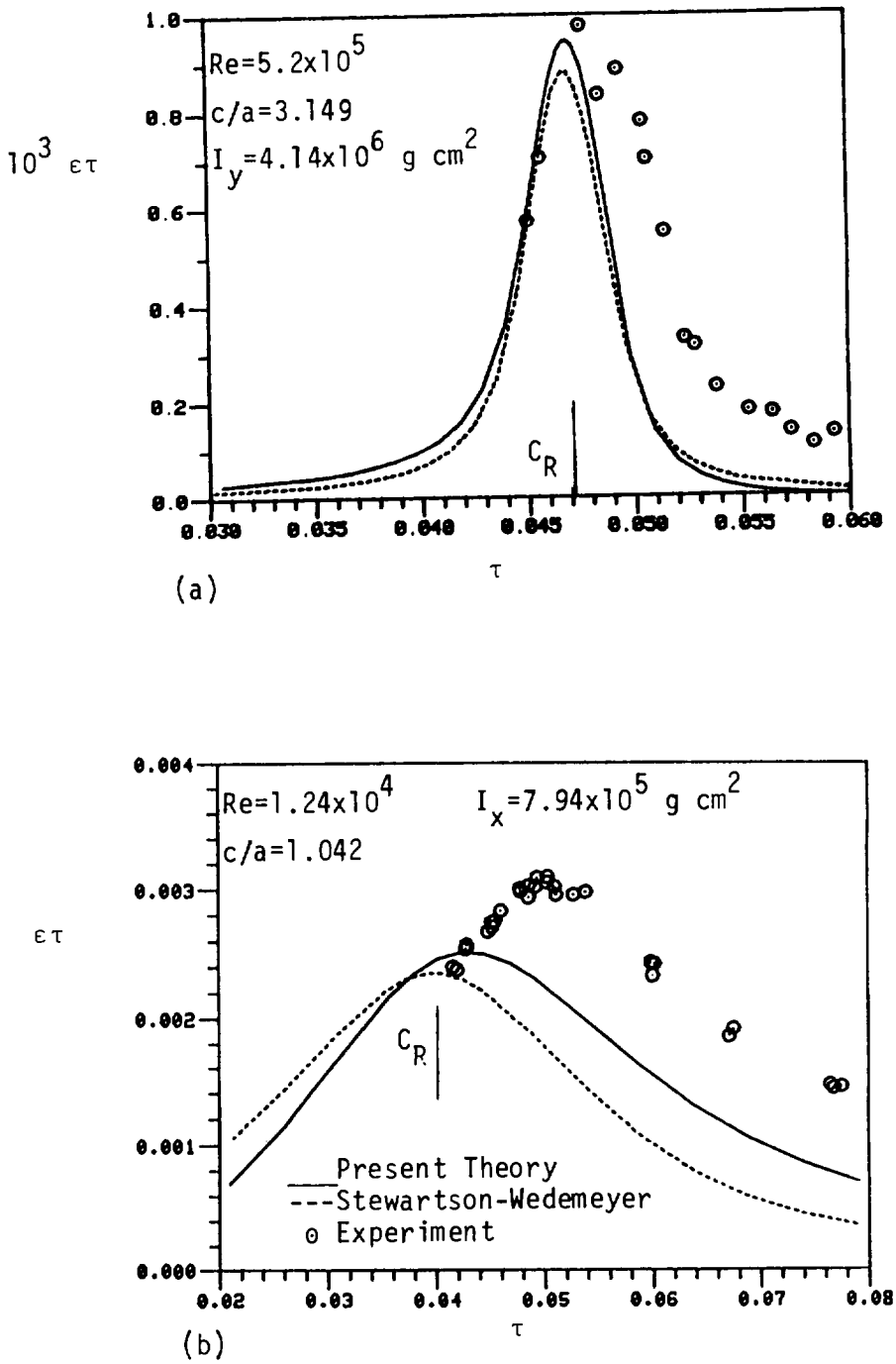

Figure 8. Comparison of Theoretical and Experimental Yaw Growth Rates ($\hat{M}$=0.0, ℓ=0.0): (a) a=3.153 cm, ρ=0.818 g/cm^3; (b) a=6.359 cm, ρ=0.966 g/cm^3.

LIST OF SYMBOLS

a	cross-sectional radius of cylinder [cm]
a_k	least-squares coefficients for series of axial eigenfunctions, Eq. (42)
b_k	biorthogonal coefficients for series of axial eigenfunctions, Eq. (40)
c	half-height of cylinder
$\bar{c}$	$\equiv c/a$, aspect ratio
C_p	perturbation pressure coefficient, Eq. (51)
C_I	natural oscillation decay-rate of rotating liquid/$\dot{\phi}$
C_R	natural oscillation frequency of rotating liquid/$\dot{\phi}$
C_{LM}	liquid moment coefficient = $C_{LSM} + i\, C_{LIM}$, Eq. (5)
C_{LIM}	liquid in-plane moment coefficient, Eqs. (6) and (60)
C_{LSM}	liquid side moment coefficient, Eqs. (6) and (60)
Dp	disturbance pressure = $p-(\frac{1}{2})\bar{r}^2$, Eq. (48), [pressure/$\rho a^2\dot{\phi}^2$]
f	$\equiv(1-i\varepsilon)\tau$, complex representation of angular motion Eq. (4)
I_x	moment of inertia of empty shell about its longitudinal axis
I_y	transverse moment of inertia of empty shell about its center of gravity
k	index of axial eigenfunction and eigenvalue, Eqs. (28) and (31)
K_o	yaw amplitude at time t = 0
K_1	$\equiv K_o e^{\varepsilon\tau\dot{\phi}t}$, yaw amplitude at time t, Eqs. (3) and (4)

ℓ	x (and $\tilde{x}$) coordinate of pivot point
m_L	mass of liquid in cylinder = $2\pi\rho a^2 c$ [g]
$M_{L\tilde{Y}}$, $M_{L\tilde{Z}}$	$\tilde{y}$ and $\tilde{z}$ components, respectively of liquid moment [g cm^2/s^2]
$M_{L\tilde{Z}S}$, $M_{L\tilde{Z}E}$	sidewall and endwall contributions, respectively, to $M_{L\tilde{Z}}$
$M_{L\tilde{Z}T}$, $M_{L\tilde{Z}B}$	top and bottom wall contributions, respectively, to $M_{L\tilde{Z}}$
M_1, M_2	non-dimensional liquid moment coefficients, in-plane and side plane, respectively, Eq. (58)
M_{1E}, M_{2E}	endwall contributions to M_1 and M_2, Eqs. (56), (57c), (57d), (59)
M_{1S}, M_{2S}	sidewall contributions to M_1 and M_2, Eqs. (56), (57a), (57b), (59)
$\hat{M}$	aerodynamic (or gravity) moment parameter, Eq. (2) [s^{-2}]
n_{YE}, n_{ZE}	components of the projection in the y, z plane of a unit vector along projectile axis
p	pressure/$(\rho a^2\dot{\phi}^2)$
$\underline{p} \equiv \underline{p}_R + i\,\underline{p}_I$	non-dimensional r, x variation of perturbation pressure, Eq. (17d), [pressure/$(K_o\rho a^2\dot{\phi}^2)$]
$\underline{p}_H$	series solution contribution to $\underline{p}$, Eq. (28)
$\underline{p}_p$	particular solution contribution to $\underline{p}$, Eq. (22)
p^*	perturbation pressure/$(K_o\rho a^2\dot{\phi}^2)$, Eq. (10)
$\hat{p}_k(r)$	coefficient of $\sin \lambda_k x$ in $\underline{p}_H$ series, Eq. (28)
P	unperturbed pressure/$(\rho a^2\dot{\phi}^2)$, Eqs. (10) and (11)
P_1, P_2	perturbation pressure coefficients, Eq. (50), [pressure/$(K_o\rho a^2\dot{\phi}^2)$]
r	radial coordinate in inertial system/a

$\tilde{r}$	radial coordinate in non-rotating aeroballistic system/a
$R_1, \ldots, R_4$	functions of radial variation in separated flow solutions $\underline{u}_H$, $\underline{v}_H$, $\underline{w}_H$, $\underline{p}_H$, respectively, Eqs. (26) and (C.1)
Re	Reynolds number = $a^2 \dot{\phi}/\nu$
t	time [s]
$\bar{t}$	$= \dot{\phi}t$
u, v, w	non-dimensional radial, azimuthal, and axial velocity components, respectively, in inertial system [velocity/($\dot{\phi}$a)]
$\underline{u}$, $\underline{v}$, $\underline{w}$	non-dimensional x, r variation of perturbation velocity components, Eq. (17) [velocity/($K_o\dot{\phi}$a)]
$\underline{u}_H$, $\underline{v}_H$, $\underline{w}_H$	series solution contribution to $\underline{u}$, $\underline{v}$, $\underline{w}$, Eq. (28)
$\underline{u}_p$, $\underline{v}_p$, $\underline{w}_p$	particular solution contribution to $\underline{u}$, $\underline{v}$, $\underline{w}$, Eq. (22)
u^*, v^*, w^*	non-dimensional perturbation velocity components in inertial system, Eqs. (10) and (A1) [velocity/($K_o\dot{\phi}$a)]
$\tilde{u}$, $\tilde{v}$, $\tilde{w}$	non-dimensional radial, azimuthal, and axial velocity components, respectively, in aeroballistic system [velocity/($\dot{\phi}$a)]
$\tilde{u}^*, \tilde{v}^*, \tilde{w}^*$	non-dimensional perturbation velocity components in aeroballistic system, Eq. (A.1) [velocity/($K_o\dot{\phi}$a)]
$\hat{u}_k$, $\hat{v}_k$, $\hat{w}_k$	coefficients of $\sin\lambda_k x$ and $\cos\lambda_k x$ in $\underline{u}_H$, $\underline{v}_H$, $\underline{w}_H$ series, Eq. (28)
U, V, W	non-dimensional radial, azimuthal, and axial velocity components of unperturbed flow, Eq. (11) [velocity/($\dot{\phi}$a)]
$X_1, \ldots, X_4$	functions of axial variation in separated flow solutions $\underline{u}_H$, $\underline{v}_H$, $\underline{w}_H$, $\underline{p}_H$, respectively, Eqs. (26) and (C1)
x, y, z	non-dimensional rectangular coordinates in inertial system (x-axis along trajectory) [length/a]
$\tilde{x}$, $\tilde{y}$, $\tilde{z}$	non-dimensional rectangular coordinates in aeroballistic system ($\tilde{x}$-axis along cylinder axis) [length/a]

$y_1, \ldots y_6$	functions describing radial variation of perturbation flow variables, Eqs. (34) and (35)
$\tilde{\alpha}$	angle in vertical plane measured from the $\tilde{x}$-axis to the velocity vector
$\tilde{\beta}$	angle in horizontal plane measured from the $\tilde{x}$-axis to the velocity vector
δc	correction term in endwall boundary condition, Eqs. (29) and (30)
ε	= $(1/\tau)$ × yaw growth per radian of nutation
$\theta, \tilde{\theta}$	polar angles in inertial and aeroballistic systems, respectively, Eqs. (7) and (8)
λ	separation of variables constant, Eq. (27)
λ_k	eigenvalue in the axial problem, Eqs. (28) and (31)
ν	kinematic viscosity of liquid [cm²/s]
$\tilde{\xi}$	vector describing angular motion of cylinder, Eq. (1)
ρ	density of liquid [g/cm³]
τ	nutational frequency of cylinder/$\dot{\phi}$
ϕ_1	= $\tau\dot{\phi}t$, angular orientation of $\tilde{x}$-axis in the x, y, z system
$\dot{\phi}$	spin rate of cylinder [rad/s], taken to be positive

APPENDIX A. DERIVATION OF WALL BOUNDARY CONDITIONS

The wall boundary conditions, Eq. (15), must be restated in terms of $\overset{*}{u}$, $\overset{*}{v}$, $\overset{*}{w}$ at $r = 1$ and $x = \pm\tilde{c}$. Recalling the definitions of Eqs. (10) and (11),

$$
\begin{aligned}
u = dr/d\bar{t} &= -K_o \overset{*}{u}, \qquad & v = r\, d\theta/d\bar{t} &= r\text{-}K_o \overset{*}{v}, \\
& & w = dx/d\bar{t} &= -K_o \overset{*}{w} \\
\tilde{u} = d\tilde{r}/d\bar{t} &= -K_o \overset{*}{\tilde{u}}, \qquad & \tilde{v} = \tilde{r}\, d\tilde{\theta}/d\bar{t} &= \tilde{r}\text{-}K_o \overset{*}{\tilde{v}}, \\
& & \tilde{w} = d\tilde{x}/d\bar{t} &= -K_o \overset{*}{\tilde{w}},
\end{aligned}
\tag{A1}
$$

where $\bar{t} \equiv \dot{\phi} t$.

The velocity transformation between earth-fixed and aeroballistic systems is obtained by differentiating Eq. (9) with respect to time and substituting the expressions of Eq. (A 1) for the derivatives:

$$
\begin{aligned}
\overset{*}{u} &= \overset{*}{\tilde{u}} - (\tilde{x}-\ell) e^{\varepsilon\tau\dot{\phi}t} [\varepsilon\tau \cos(\phi_1 - \tilde{\theta}) + (1-\tau) \sin(\phi_1 - \tilde{\theta})] + O(K_o) \\
\overset{*}{v} &= \overset{*}{\tilde{v}} - (\tilde{x}-\ell) e^{\varepsilon\tau\dot{\phi}t} [-(1-\tau) \cos(\phi_1 - \tilde{\theta}) + \varepsilon\tau \sin(\phi_1 - \tilde{\theta})] + O(K_o) \\
\overset{*}{w} &= \overset{*}{\tilde{w}} - \tilde{r}\, e^{\varepsilon\tau\dot{\phi}t} [-\varepsilon\tau \cos(\phi_1 - \tilde{\theta}) - (1-\tau) \sin(\phi_1 - \tilde{\theta})] + O(K_o).
\end{aligned}
\tag{A2}
$$

The tilde superscripts can be dropped from the bracketed terms of Eq. (A2) without changing the order of error.

We now evaluate Eq. (A2) at $r = 1$, applying the conditions $\overset{*}{\tilde{u}}(\tilde{r}=1) = \overset{*}{\tilde{v}}(\tilde{r}=1) = \overset{*}{\tilde{w}}(\tilde{r}=1) = 0$. Thus,

$$
\begin{aligned}
\overset{*}{u}(r=1) &= \overset{*}{\tilde{u}}(\tilde{r}=1) + (\tilde{r}_{r=1} - 1)\, (\partial\tilde{u}/\partial\tilde{r})_{r=1} \\
&= 0 + K_o e^{\varepsilon\tau\dot{\phi}t} (x-\ell) \cos(\phi_1 - \theta)\, (\partial\overset{*}{\tilde{u}}/\partial\tilde{r})_{r=1}.
\end{aligned}
\tag{A3}
$$

Similar expressions apply to $\overset{*}{v}(r=1)$ and $\overset{*}{w}(r=1)$. The coefficients of the first order terms (in K_o) contain gradients which might be large at $r = 1$ when the Reynolds number is large. However, at this stage we are only

considering perturbations from the point of view of the small parameter K_o. Hence, to zeroth order,

$$\overset{*}{\underset{\sim}{u}}(r=1) = \overset{*}{\underset{\sim}{v}}(r=1) = \overset{*}{\underset{\sim}{w}}(r=1) = 0, \text{ and consequently}$$

$$\begin{aligned}
\overset{*}{u}(r=1) &= -(x-\ell)e^{\varepsilon\tau\dot{\phi}t}[\varepsilon\tau\cos(\phi_1-\theta) + (1-\tau)\sin(\phi_1-\theta)] \\
\overset{*}{v}(r=1) &= -(x-\ell)e^{\varepsilon\tau\dot{\phi}t}[-(1-\tau)\cos(\phi_1-\theta) + \varepsilon\tau\sin(\phi_1-\theta)] \\
\overset{*}{v}(r=1) &= -e^{\varepsilon\tau\dot{\phi}t}[-\varepsilon\tau\cos(\phi_1-\theta) - (1-\tau)\sin(\phi_1-\theta)].
\end{aligned} \tag{A4}$$

Similar consideration applied to the endwalls leads to the conclusion that $\overset{*}{\underset{\sim}{u}}(x=\pm\underset{=}{c}) = \overset{*}{\underset{\sim}{v}}(x=\pm\underset{=}{c}) = \overset{*}{\underset{\sim}{w}}(x=\pm\underset{=}{c}) = 0 + O(K_o)$; Eqs. (A2) now yield

$$\begin{aligned}
\overset{*}{u}(x=\pm\underset{=}{c}) &= -(\pm\underset{=}{c}-\ell)e^{\varepsilon\tau\dot{\phi}t}[+\varepsilon\tau\cos(\phi_1-\theta) + (1-\tau)\sin(\phi_1-\theta)] \\
\overset{*}{v}(x=\pm\underset{=}{c}) &= -(\pm\underset{=}{c}-\ell)e^{\varepsilon\tau\dot{\phi}t}[-(1-\tau)\cos(\phi_1-\theta) + \varepsilon\tau\sin(\phi_1-\theta)] \\
\overset{*}{w}(x=\pm\underset{=}{c}) &= -r\,e^{\varepsilon\tau\dot{\phi}t}[-\varepsilon\tau\cos(\phi_1-\theta) - (1-\tau)\sin(\phi_1-\theta)].
\end{aligned} \tag{A5}$$

APPENDIX B. AXIAL BOUNDARY CONDITIONS

The first of Eqs. (20), namely, $\underline{u}-i\underline{v} = 0$ at r=0, is obtained merely by setting r=0 in Eq. (18a). The next condition, namely, $\underline{w}(r=0) = 0$, is obtained by multiplying Eq. (18d) by r^2, then setting r=0.

If one differentiates Eq. (18a) with respect to r, then sets r = 0 (remembering that $\underline{w}_x(r=0) = 0$ because $\underline{w}(r=0) = 0$), one obtains

$$2\underline{u}_r(r=0)-i\underline{v}_r(r=0) = 0. \tag{B1}$$

If one multiplies Eq. (18c) by r^2, differentiates with respect to r, then sets r=0, one obtains

$$i\underline{p}(r=0)+(1/Re)[-\underline{v}_r(r=0)-2i\underline{u}_r(r=0)] = 0. \tag{B2}$$

Application of Eq. (B1) here leads to the third condition, namely,

$$\underline{p}(r=0) = 0. \tag{B3}$$

Alternatively, the boundary conditions at r=0 can be derived only on the basis of continuity and single-valuedness.[5]

APPENDIX C. SEPARATION OF VARIABLES IN THE LINEARIZED NAVIER-STOKES EQUATIONS

Our perturbation equations follow directly from the linearized Navier-Stokes equations. After the t and θ variations are removed, as in Eqs. (17), the perturbation equations are in the form of Eqs. (18). The form of the solution to these equations was obtained by separation of variables. Since this procedure cannot be carried out strictly in the usual manner, it is outlined here.

The variables are separated as in Eq. (26) and substituted into Eqs. (18). The manipulations will be outlined only for Eq. (18b) since the others are treated in the same way. After collecting terms, Eq. (18b) becomes

$$\begin{aligned}&[\mathrm{Re}^{-1}(R_1'' + R_1'/r - 2R_1/r^2) - i(f-1)]\ X_1 + \\ &\qquad \mathrm{Re}^{-1} R_1 X_1'' + 2\ [\mathrm{Re}^{-1}\ i/r^2 + 1]\ R_2 X_2 - R_4' X_4 = 0,\end{aligned} \tag{C1}$$

where the prime indicates differentiation with respect to the argument. It is convenient to denote each coefficient of the functions of x by a single symbol. Thus Eq. (C1) is rewritten as

$$g_1(r)\ X_1 + g_2(r)\ X_1'' + g_3(r)\ X_2 - g_4(r)\ X_4 = 0. \tag{C2}$$

Divide this by g_4 and differentiate with respect to r to obtain

$$(g_1/g_4)'\ X_1 + (g_2/g_4)'\ X_1'' + (g_3/g_4)'\ X_2 = 0.$$

Next, divide by $(g_3/g_4)'$ and differentiate with respect to r. This gives

$$[(g_1/g_4)'/(g_3/g_4)']'\ X_1 + [(g_2/g_4)'/(g_3/g_4)']'\ X_1'' = 0. \tag{C3}$$

The usual argument employed in separating variables shows that

$$X_1'' = \text{const.}\ X_1,$$

which is the form given in Eq. (27).

The same process applied to Eqs. (18d) and (18a) yields

$$X_3'' = \text{const.}\ X_3$$

and

$$X_2 = \text{const.}\ X_1 ,$$

respectively. When the above three results are substituted into Eq. (C2), the result is

$$X_4 = \text{const.}\ X_1 .$$

The boundary conditions dictate the solution to the harmonic equations, as shown in Eq. (28). The particular solution stated in Eqs. (22) is obtained by setting equal to zero the constants of $X_i''/X_i = \text{constant}$.

APPENDIX D. THE ENDWALL BOUNDARY CONDITION

After various transformations, the flow problem to be solved is given by Eq. (18), the linearized Navier-Stokes equation, plus the boundary conditions on the axis, Eq. (25), on the sidewall, Eq. (23), and the endwalls, Eq. (24). The method of solution adopted is separation of variables in order to get the normal modes. The axial and sidewall boundary conditions can be satisfied with the modal solution, but only the condition of no flow through the end wall, Eq.(24c), can be satisfied there. The remaining no slip conditions, Eq. (24a, b), cannot be satisfied. Rather than the viscous boundary conditions, we satisfy the condition $\underline{w}_H = 0$ that would be imposed for an inviscid fluid and accept the values of $\underline{u}_H$ and $\underline{v}_H$ on the endwalls from the solution, as in an inviscid flow.

The proper normal modes are obtained only for λ real in Eq. (27). However, the modal solution is inconsistent with the linearized Navier-Stokes equations and the no slip boundary conditions. Since we have had to drop two of the three endwall conditions, we can conjecture that a boundary layer must be inserted in order to satisfy these. This is what Wedemeyer[3] did to correct the inviscid solution of Stewartson[1]. This is the type of correction needed here. It is done in the same spirit as Wedemeyer's correction but must be derived as a correction to Eqs. (18) which are not Stewartson's inviscid equations.

The technique of matched asymptotic expansions is used here since it provides a systematic method of handling this type of singular perturbation problem; the results are more easily interpreted than in Wedemeyer's approach, and some difficulties in his approach are avoided. The technique is described by Van Dyke[11]. However, the way the technique is applied is tailored to the particular problem we solve.

To avoid a proliferation of indices, the notation is changed for this Appendix only. The sub-bar and sub-H are dropped, see Eq. (21), and we let $C \equiv \bar{\bar{c}}$. The flow variables are now u, v, w, and p. The linear Eqs. (18) are written with the linear operator.

$$L(u, v, w, p) = 0. \tag{D1}$$

Only the boundary conditions at x = C are needed in this derivation:

$$\begin{aligned} u &= ig \\ v &= g \qquad \text{at } x = C \\ w &= 0 \\ g &= -\,[2f\,(1-f)/(1+f)]\,C \end{aligned} \tag{D2}$$

---

11. *M. Van Dyke, Perturbation Methods in Fluid Mechanics, Academic Press, New York, N.Y., 1964.*

The asymptotic solution to Eq. (D1) with Eq. (D2) for $Re \to \infty$ is obtained by constructing inner and outer solutions with appropriately scaled inner and outer variables. The outer variables are unchanged, which conforms with Eq. (18). The outer solution has the asymptotic form

$$\begin{aligned} u &\sim u_o\,(x, r, Re) + \Delta_1\,(Re)\,u_{o1}\,(x, r, Re) + \ldots \\ v &\sim v_o\,(x, r, Re) + \Delta_2\,(Re)\,v_{o1}\,(x, r, Re) + \ldots \\ w &\sim w_o\,(x, r, Re) + \Delta_3\,(Re)\,w_{o1}\,(x, r, Re) + \ldots \\ p &\sim p_o\,(x, r, Re) + \Delta_4\,(Re)\,p_{o1}\,(x, r, Re) + \ldots \end{aligned} \tag{D3}$$

where $\Delta_j \to 0$ as $Re \to \infty$, and this form is valid for $Re \to \infty$ with x and r fixed. For the inner solution x is replaced by $y = C - x$, and inner variables

$$\begin{aligned} \bar{y} &= y/\varepsilon\,(Re) \\ \bar{r} &= r \end{aligned} \tag{D4}$$

are introduced where $\varepsilon \to 0$ as $Re \to \infty$; in this Appendix super-bar does <u>not</u> denote complex conjugate. The inner solution has the asymptotic form

$$\begin{aligned} u &\sim \delta_1\,u_i\,(\bar{y}, \bar{r}) + \delta_{11}\,u_{i1}\,(\bar{y}, \bar{r}) + \ldots \\ v &\sim \delta_2\,v_i\,(\bar{y}, \bar{r}) + \delta_{21}\,v_{i1}\,(\bar{y}, \bar{r}) + \ldots \\ w &\sim \delta_3\,w_i\,(\bar{y}, \bar{r}) + \delta_{31}\,w_{i1}\,(\bar{y}, \bar{r}) + \ldots \\ p &\sim \delta_4\,p_i\,(\bar{y}, \bar{r}) + \delta_{41}\,p_{i1}\,(\bar{y}, \bar{r}) + \ldots \end{aligned} \tag{D5}$$

where $\delta_j \to 0$ as $Re \to \infty$, $\delta_{j1} \ll \delta_j$, and the form is valid for $Re \to \infty$ with $\bar{y}$ and $\bar{r}$ fixed.

The scales Δ_j, δ_j, δ_{j1} and ε must be determined from matching the inner and outer solutions and from whatever information the problem provides. However, the terms in Eq. (D3), $u_o\,(x, r, Re)$, etc., and $u_{o1}\,(x, r, Re)$, etc., are not in proper form for matching because they are functions of Re. This follows from the fact that the first terms satisfy

$$L\,(u_o,\ v_o,\ w_o,\ p_o) = 0 \tag{D6}$$

and similarly for the second terms u_{o1}, etc. Matching requires that the only dependence on Re be in the scales Δ_j. The terms of Eq. (D3) can also be expanded in asymptotic series:

$$u_o \sim u_o{}^o\,(x,\ r) + Re^{-1}\,u_o{}^1\,(x,\ r) + \ldots \tag{D7}$$

etc.

and

$$u_{o1} \sim u_{o1}{}^o\,(x,\ r,) + Re^{-1}\,u_{o1}{}^1\,(x,\ r) + \ldots, \tag{D8}$$

the form of the expansion being determined by Eq. (D6). The functions $u_o{}^o$ etc., and $u_{o1}{}^o$, etc, satisfy the inviscid equations and are not functions of Re; $u_o{}^1$, etc., and $u_{o1}{}^1$, etc., satisfy a non-homogeneous form of the inviscid equations. This explains why we can get a solution with only the one boundary condition on normal velocity. The process described in this paragraph is tailored to the problem we solve; a more direct approach would normally be used.

The asymptotic matching principle[11] can now be applied. Only the results are given:

$$\varepsilon = Re^{-1/2}$$

$$\delta_1 = \delta_2 = \delta_4 = 1 \qquad \Delta_j = Re^{-1/2},\ j = 1,\ 2,\ 3,\ 4$$

$$\delta_3 = Re^{-1/2}$$

The first terms in Eq. (D5) satisfy the boundary layer equations:

$$\begin{aligned}
&i\,(f - 1)\,u_i - 2v_i = -\,p_{i\,\bar{r}} + u_{i\,\bar{y}\,\bar{y}} \\
&i\,(f - 1)\,v_i + 2u_i = i\,p_i/\bar{r} + v_{i\,\bar{y}\,\bar{y}} \\
&p_{i\,\bar{y}} = 0 \\
&(\bar{r}\,u_i)_{\bar{r}} - i\,v_i - \bar{r}\,w_{i\,\bar{y}} = 0
\end{aligned} \tag{D9}$$

with boundary conditions on the endwall, obtained from Eq. (D2),

$$u_i\ (0,\ \bar{r}) = ig$$

$$v_i\ (0,\ \bar{r}) = g$$

$$w_i\ (0,\ \bar{r}) = 0$$

and at the edge of the boundary layer, obtained from matching,

$$u_i\ (\infty,\ \bar{r}) = u_o^{\,o}\ (C,\ r)$$

$$v_i\ (\infty,\ \bar{r}) = v_o^{\,o}\ (C,\ r)$$

$$p_i\ (\infty,\ \bar{r}) = p_o^{\,o}(C,\ r)$$

or more generally $p_i(\bar{y},\ \bar{r}) = p_o^{o}\ (C,\ r)$. No condition on $w_i(\infty,\ \bar{r})$ is obtained or allowed. The solution to Eq. (D9) is easily obtained and is required in the matching.

The boundary condition, Eq. (29a), must be interpreted as a condition on the outer solution which is given by

$$w \sim w_o^{\,o}\ (x,\ r) + Re^{-1/2}\ w_{o1}^{\,o}\ (x,\ r) + 0\ (Re^{-1}) \tag{D10}$$

The functions here satisfy only one boundary condition on the wall:

$$\begin{aligned} w_o^{\,o}\ (C,\ r) &= 0 \\ w_{o1}^{\,o}\ (C,\ r) &= Re^{1/2}\ \delta c\ \left.\frac{\partial w_o^{\,o}}{\partial x}\right|_{x\,=\,C} \end{aligned} \tag{D11}$$

the latter being obtained by matching. Using Eqs. (D11) and (D10) we obtain

$$w - \delta c\ w_x = 0 + 0\ (Re^{-1}) \text{ at } x = C, \tag{D12}$$

which is Eq. (29a). This development shows that, rather than solving Eq. (D1), we could solve two inviscid type problems with boundary conditions Eq. (D11) and combine them linearly to get Eq. (D10). Actually this is not practical because the radial variation and no slip conditions at the sidewall must be found.

The above asymptotic solution was obtained using two terms in the outer solution and one term in the inner solution. To obtain the next approximation to the boundary condition, three terms in the outer and two terms in the inner would be necessary. The boundary condition will have an error $0\ (Re^{-3/2})$ and should allow a more accurate solution for lower Re.

APPENDIX E. THE BIORTHOGONAL EXPANSION

Separation of variables leads to the result that the X_i in Eq. (26) satisfys the harmonic equation, Eq. (27), where λ is a separation constant. Considering $\underline{w}_H$ and applying the boundary conditions (29) yield the following boundary value problem, assuming $\ell=0$,

$$
\begin{aligned}
&Z'' + \lambda^2 Z = 0 \\
&Z'(-\bar{\bar{c}}) - \lambda^2 \delta c\, Z(-\bar{\bar{c}}) = 0 \\
&Z'(\bar{\bar{c}}) + \lambda^2 \delta c\, Z(\bar{\bar{c}}) = 0
\end{aligned}
\tag{E1}
$$

where $X_3(x)$ is replaced by $Z'(x)$ because we wish to develope the expansion for x needed in Eq. (38). The eigenvalue, λ, is determined from

$$
(1-\delta c^2 \lambda_j^2) \sin 2\lambda_j \bar{\bar{c}}_j = 2\bar{\bar{c}}\lambda_j \cos 2\lambda_j \bar{\bar{c}}_j \tag{E2}
$$

which can be split into two equations, one of which is Eq. (31) and is the appropriate one for our problem. A denumerable set of complex solutions, λ_j, exists. Even though the differential equation in (E1) is self-adjoint, the system (E1) is not, which means that complex eigenvalues are to be expected. The non self-adjoint problem and the presence of the eigenvalue in the boundary conditions make this a nonstandard problem. The eigenfunctions are not orthogonal and several of the usual results for expansion of a function in a series of eigenfunctions do not apply.

This type of problem can be attacked by introducing the adjoint problem:

$$
\begin{aligned}
&Y'' + \bar{\lambda}^2 Y = 0 \\
&Y'(-\bar{\bar{c}}) - \bar{\lambda}^2\, \overline{\delta c}\, Y(-\bar{\bar{c}}) = 0 \\
&Y'(\bar{\bar{c}}) + \bar{\lambda}^2 \overline{\delta c}\, Y(\bar{\bar{c}}) = 0
\end{aligned}
\tag{E3}
$$

where - denotes complex conjugate.

An essential part of the theory for the expansion of a function in a series of eigenfunctions is the proper definition of an inner product. In this problem solutions Z_j (eigenvalue λ_j) to Eq. (E1) and Y_k (eigenvalue $\bar{\lambda}_k$) to Eq. (E3) are needed to define the inner product (Z_j, Y_k). It can be shown that the inner product must be defined as

$$(Z_j, Y_k) \equiv \int_{-\bar{\bar{c}}}^{\bar{\bar{c}}} Z_j \bar{Y}_k \, dx - \delta c[Z_j(\bar{\bar{c}})\, \bar{Y}_k(\bar{\bar{c}}) + Z_j(-\bar{\bar{c}})\, \bar{Y}_k(-\bar{\bar{c}})].$$

The boundary terms in this expression arise from the presence of λ in the boundary conditions. The functions Z_j and Y_k are biorthogonal if

$$(Z_j, Y_k) = 0.$$

Any solution Z_j is biorthogonal to any solution Y_k if $j \neq k$. However, Z_j and Z_k or Y_j and Y_k are not biorthogonal.

A more or less arbitrary function can be expanded in terms of the eigenfunctions, Z_j, (or equivalently Y_j)

$$f = \sum_{j=1}^{\infty} C_j Z_j$$

where $C_k = (f, Y_k)/(Z_k, Y_k)$

with all the usual desirable properties. In particular the function x can be expanded as in Eq. (39) with the coefficients b_k given in Eq. (40).

DISTRIBUTION LIST

No. of Copies	Organization
12	Administrator Defense Technical Info Center ATTN: DTIC-DDA Cameron Station Alexandria, VA 22314
1	Commander US Army Engineer Waterways Experiment Station ATTN: R.H. Malter Vicksburg, MS 39180
1	Commander US Army Materiel Development and Readiness Command ATTN: DRCDMD-ST 5001 Eisenhower Avenue Alexandria, VA 22333
4	Commander US Army Armament Research and Development Command ATTN: DRDAR-TSS (2 cys) DRDAR-LC, Dr. J. Fraiser DRDAR-TDC, Dr. D. Gyorog Dover, NJ 07801
6	Commander US Army Armament Research and Development Command ATTN: DRDAR-LCA-F Mr. D. Mertz Mr. E. Falkowski Mr. A. Loeb Mr. R. Kline Mr. S. Kahn Mr. S. Wasserman Dover, NJ 07801
1	Commander US Army Armament Materiel Readiness Command ATTN: DRSAR-LEP-L, Tech Lib Rock Island, IL 61299

No. of Copies	Organization
1	Director US Army ARRADCOM Benet Weapons Laboratory ATTN: DRDAR-LCB-TL Watervliet, NY 12189
1	Commander US Army Aviation Research and Development Command ATTN: DRDAV-E 4300 Goodfellow Blvd St. Louis, MO 63120
2	Director US Army Air Mobility Research and Development Laboratory ATTN: SAVDL-D, W.J. McCroskey Ames Research Center Moffett Field, CA 94035
1	Commander US Army Communications Research and Development Command ATTN: DRDCO-PPA-SA Fort Monmouth, NJ 07703
1	Commander US Army Electronics Research and Development Command Technical Support Activity ATTN: DELSD-L Fort Monmouth, NJ 07703
1	Commander US Army Missile Command ATTN: DRSMI-R Redstone Arsenal, AL 35898
1	Commander US Army Missile Command ATTN: DRSMI-YDL Redstone Arsenal, AL 35898
1	Commander US Army Missile Command ATTN: DRSMI-RDK, Mr. R. Deep Restone Arsenal, AL 35898

DISTRIBUTION LIST

No. of Copies	Organization
1	Commander US Army Tank Automotive Research & Development Command ATTN: DRDTA-UL Warren, MI 48090
1	Commander US Army Jefferson Proving Ground ATTN: STEJP-TD-D Madison, IN 47251
1	Commander US Army Research Office ATTN: Dr. R.E. Singleton P.O. Box 12211 Research Triangle Park, NC 27709
1	AGARD-NATO ATTN: R.H. Korkegi APO New York 09777
1	Director US Army TRADOC Systems Analysis Activity ATTN: ATAA-SL, Tech Lib White Sands Missile Range NM 88002
3	Commander Naval Air Systems Command ATTN: AIR-604 Washington, DC 20360
2	Commander David W. Taylor Naval Ship Research & Development Center ATTN: H.J. Lugt, Code 1802 S. de los Santos, Head, High Speed Aero Division Bethesda, MD 20084
1	Commander Naval Surface Weapons Center ATTN: DX-21, Lib Br Dahlgren, VA 22448
5	Commander Naval Surface Weapons Center Applied Aerodynamics Division ATTN: K.R. Enkenhus M. Ciment S.M. Hastings A.E. Winklemann W.C. Ragsdale Silver Spring, MD 20910
1	AFATL (DLDL, Dr. D.C.Daniel) Eglin AFB, FL 32542
2	AFFDL (W.L. Hankey; J.S. Shang) Wright-Patterson AFB, OH 45433
4	Director National Aeronautics and Space Administration ATTN: D.R. Chapman J. Rakich W.C. Rose B. Wick Ames Research Center Moffett Field, CA 94035
4	Director National Aeronautics and Space Administration ATTN: E. Price J. South J.R. Sterrett Tech Library Langley Research Center Langley Station Hampton, VA 23365
1	Director National Aeronautics and Space Administration Lewis Research Center ATTN: MS 60-3, Tech Lib 21000 Brookpark Road Cleveland, OH 44135

DISTRIBUTION LIST

No. of Copies	Organization
2	Director National Aeronautics and Space Administration Marshall Space Flight Center ATTN: A.R. Felix, Chief S&E-AERO-AE Dr. W.W. Fowlis Huntsville, AL 35812
2	Director Jet Propulsion Laboratory ATTN: L.M. Mach Tech Library 4800 Oak Grove Drive Pasadena, CA 91103
3	Arnold Research Org., Inc. ATTN: J.D. Whitfield R.K. Matthews J.C. Adams Arnold AFB, TN 37389
3	Aerospace Corporation ATTN: H. Mirels R.L. Varwig Aerophysics Lab. P.O. Box 92957 Los Angeles, CA 90009
1	AVCO Systems Division ATTN: B. Reeves 201 Lowell Street Wilmington, MA 01887
3	Boeing Commercial Airplane Company ATTN: R. A. Day M.S. 1W-82, Org B-8120 P.E. Rubbert, MS 3N-19 J.D. McLean, MS-3N-19 Seattle, WA 98124
3	Calspan Corporation ATTN: A. Ritter G. Homicz W. Rae P.O. Box 400 Buffalo, NY 14225
1	General Dynamics ATTN: Research Lib 2246 P.O. Box 748 Fort Worth, TX 76101
1	General Electric Company, RESD ATTN: W. J. East 3198 Chestnut Street Philadelphia, PA 19101
2	Grumman Aerospace Corporation ATTN: R.E. Melnik L.G. Kaufman Bethpage, NY 11714
2	Lockheed-Georgia Company ATTN: B.H. Little, Jr. G.A. Pounds Dept 72074, Zone 403 86 South Cobb Drive Marietta, GA 30062
1	Lockheed Missiles and Space Company ATTN: Tech Info Center 3251 Hanover Street Palo Alto, CA 94304
3	Martin-Marietta Laboratories ATTN: S.H. Maslen S.C. Traugott H. Obremski 1450 S. Rolling Road Baltimore, MD 21227
2	McDonnell Douglas Astronautics Corporation ATTN: J. Xerikos H. Tang 5301 Bolsa Avenue Huntington Beach, CA 92647

DISTRIBUTION LIST

No. of Copies	Organization
2	McDonnell-Douglas Corporation Douglas Aircraft Company ATTN: T. Cebeci K. Stewartson 3855 Lakewood Boulevard Long Beach, CA 90801
2	Sandia Laboratories ATTN: F.G. Blottner Tech Lib. Albuquerque, NM 87115
2	United Aircraft Corporation Research Laboratory ATTN: M.J. Werle Library East Hartford, CT 06108
1	LTV Aerospace Corp. Vought Systems Division ATTN: J.M. Cooksey, Chief, Gas Dynamics Lab, 2-53700 P.O. Box 5907 Dallas, TX 75222
1	Arizona State University Department of Mechanical and Energy Systems Engineering ATTN: G.P. Neitzel Tempe, AZ 85281
3	California Institute of Technology ATTN: Tech Library H.B. Keller Mathematics Dept. D. Coles Aeronautics Dept. Pasadena, CA 91102
1	Cornell University Graduate School of Aero Engr ATTN: Library Ithaca, NY 14850
1	Illinois Institute of Tech ATTN: H. M. Nagib 3300 South Federal Chicago, IL 60616
1	The Johns Hopkins University Department of Mechanics and Materials Science ATTN: S. Corrsin Baltimore, MD 21218
4	Director Applied Physics Laboratory The Johns Hopkins University ATTN: Dr. R. D. Whiting Dr. D. A. Hurdif Dr. R. S. Hirsh Mr. E. R. Bohn Johns Hopkins Road Laurel, MD 20707
1	Louisiana State University Department of Physics and Astronomy ATTN: Dr. R.G. Hussey Baton Rouge, LA 70803
3	Massachusetts Institute of Technology ATTN: E. Covert H. Greenspan Tech Lib 77 Massachusetts Avenue Cambridge, MA 02139
2	North Carolina State Univ Mechanical and Aerospace Engineering Department ATTN: F.F. DeJarnette J.C. Williams Raleigh, NC 27607

DISTRIBUTION LIST

No. of Copies	Organization
1	Northwestern University Department of Engineering Science and Applied Mathematics ATTN: Dr. S.H. Davis Evanston, IL 60201
1	Notre Dame University Department of Aero Engr ATTN: T.J. Mueller South Bend, IN 46556
2	Ohio State University Dept of Aeronautical and Astronautical Engineering ATTN: S.L. Petrie O.R. Burggraf Columbus, OH 43210
2	Polytechic Institute of New York ATTN: G. Moretti S.G. Rubin Route 110 Farmingdale, NY 11735
3	Princeton University James Forrestal Research Ctr Gas Dynamics Laboratory ATTN: S.M. Bogdonoff S.I. Cheng Tech Library Princeton, NJ 08540
1	Purdue University Thermal Science & Prop Ctr ATTN: Tech Library W. Lafayette, IN 47907
1	Rensselaer Polytechnic Institute Department of Math Sciences ATTN: R. C. Diprima Troy, NY 12181
1	San Diego State University Department of Aerospace Engr and Engr Mechanics College of Engineering ATTN: K.C. Wang San Diego, CA 92182
1	Southern Methodist University Department of Civil and Mechanical Engineering ATTN: R.L. Simpson Dallas, TX 75275
1	Southwest Research Institute Applied Mechanics Reviews 8500 Culebra Road San Antonio, TX 78228
1	Texas A&M University College of Engineering ATTN: R.H. Page College Station, TX 77843
1	University of California - Berkeley Department of Aerospace Engineering ATTN: M. Holt Berkeley, CA 94720
1	University of California - Davis ATTN: H.A. Dwyer Davis, CA 95616

DISTRIBUTION LIST

No. of Copies	Organization
2	University of California - San Diego Department of Aerospace Engineering and Mechanical Engineering Sciences ATTN: P. Libby Tech Library La Jolla, CA 92037
1	University of Cincinnati Department of Aerospace Engineering ATTN: R.T. Davis Cincinnati, OH 45221
2	University of Colorado ATTN: E.R. Benton G.R. Inger Boulder, CO 80309
1	University of Hawaii Dept of Ocean Engineering ATTN: G. Venezian Honolulu, HI 96822
2	University of Maryland ATTN: W. Melnik J.D. Anderson College Park, MD 20742
2	University of Michigan Department of Aeronautical Engineering ATTN: W.W. Wilmarth Tech Library East Engineering Building Ann Arbor, MI 48104
1	University of Rochester Department of Mechanical and Aerospace Sciences ATTN: R. Gans Rochester, NY 14627
1	University of Santa Clara Department of Physics ATTN: R. Greeley Santa Clara, CA 95053
3	University of Southern California Department of Aerospace Engineering ATTN: T. Maxworthy P. Weidman L.G. Redekopp Los Angeles, CA 90007
1	University of Texas Department of Aerospace Engineering ATTN: J.C. Westkaemper Austin, TX 78712
1	University of Virginia Department of Aerospace Engineering & Engineering Physics ATTN: I.D. Jacobson Charlottesville, VA 22904
1	University of Washington Department of Mechanical Engineering ATTN: Tech Library Seattle, WA 98105
1	University of Wyoming ATTN: D.L. Boyer University Station Laramie, WY 82071
2	Virginia Polytechnic Institute and State University Department of Aerospace Engineering ATTN: Tech Library Dr. W. Saric Blacksburg, VA 24061

DISTRIBUTION LIST

No. of Copies	Organization
1	Woods Hole Oceanographic Institute ATTN: J.A. Whitehead Woods Hole, MA 02543

Aberdeen Proving Ground

Director, USAMSAA
ATTN: DRXSY-D
DRXSY-MP, H. Cohen

Commander, USATECOM
ATTN: DRSTE-TO-F

Commander/Director, USACSL
ATTN: Munitions Div, Bldg. E3330
E.A. Jeffers
W.C. Dee
W.J. Pribyl

Director, USACSL, Bldg. E3516, EA
ATTN: DRDAR-CLB-PA

USER EVALUATION OF REPORT

Please take a few minutes to answer the questions below; tear out this sheet, fold as indicated, staple or tape closed, and place in the mail. Your comments will provide us with information for improving future reports.

1. BRL Report Number _____

2. Does this report satisfy a need? (Comment on purpose, related project, or other area of interest for which report will be used.)

_____

_____

_____

3. How, specifically, is the report being used? (Information source, design data or procedure, management procedure, source of ideas, etc.) _____

_____

_____

4. Has the information in this report led to any quantitative savings as far as man-hours/contract dollars saved, operating costs avoided, efficiencies achieved, etc.? If so, please elaborate.

_____

_____

5. General Comments (Indicate what you think should be changed to make this report and future reports of this type more responsive to your needs, more usable, improve readability, etc.) _____

_____

_____

_____

6. If you would like to be contacted by the personnel who prepared this report to raise specific questions or discuss the topic, please fill in the following information.

Name: _____

Telephone Number: _____

Organization Address: _____

_____

_____

FOLD HERE

Director
US Army Ballistic Research Laboratory
Aberdeen Proving Ground, MD 21005

NO POSTAGE
NECESSARY
IF MAILED
IN THE
UNITED STATES

OFFICIAL BUSINESS
PENALTY FOR PRIVATE USE, $300

BUSINESS REPLY MAIL
FIRST CLASS PERMIT NO 12062 WASHINGTON, DC
POSTAGE WILL BE PAID BY DEPARTMENT OF THE ARMY

Director
US Army Ballistic Research Laboratory
ATTN: DRDAR-TSB_S
Aberdeen Proving Ground, MD 21005

FOLD HERE